

Unconventional normal-state spin dynamics in underdoped high- T_c cuprates as a fingerprint of spiral correlations of localized spins and dual localized/itinerant nature of spin fluctuations

F. Onufrieva

Laboratoire Leon Brillouin, CE-Saclay 91191 Gif-sur-Yvette, France

(Received 20 July 2015; revised manuscript received 18 January 2017; published 7 March 2017)

The paper is motivated by the observation of unusual and not well understood spin dynamics in low- and moderately doped high- T_c cuprates as well as by the discovery in these materials of a static incommensurate order for doping exceeding the insulator-metal boundary in the phase diagram. We develop a microscopic approach that allows us to treat accurately the quantum fluctuations in the spiral state developing upon doping the Mott-Neel insulator. We show that the spiral order of localized spins induces an off-diagonal order of mobile charges and a gap $\Delta \propto |\mathbf{Q}|$ in their spectrum (\mathbf{Q} is the spiral incommensurability wave vector defined with respect to \mathbf{Q}_{AF}). Due to the dynamic spin-charge interaction the latter gap produces a feedback effect consisting in the appearance of a gap in the coherent spin excitation spectrum. As a result, the characteristic energy $\omega_c = \Delta$ appears, in the spin excitation spectra. It separates two components with qualitatively different behavior—above ω_c , spin excitations are magnonlike and have an upward dispersion, below it, they are of the relaxation type and have a slight downward dispersion. The form of the dispersion is close to the form observed experimentally (by inelastic neutron scattering), which can be characterized as OPEN-hour-glass shaped or Y -shaped. There is no qualitative difference between the spin dynamics in the normal and SC states as far as doping is relatively low. There is no resonance. Other important features, including the incommensurability and uniaxial anisotropy of the low-energy spin excitations and the doping dependencies of the characteristic energy and wave vectors, are also close to those observed experimentally in low-doped cuprates. We show that the static spiral state becomes unstable at the critical doping n_c . We show also that adopting the hypothesis about the presence of finite-energy spiral correlations in the paramagnetic state above n_c and based on the results obtained for the static spiral state, it is possible to understand the spin dynamics observed in the so-called pseudogap state as well as the tendencies of the doping evolution of spin excitations in cuprates from low to high doping.

DOI: [10.1103/PhysRevB.95.125110](https://doi.org/10.1103/PhysRevB.95.125110)

I. INTRODUCTION

The theoretical description of electronic systems in a crossover between fully localized and fully itinerant electrons is a challenge in theoretical physics for a long time. A strong additional interest is stimulated by experimental advances in the field of high- T_c materials, namely of cuprates. Indeed, the high-temperature superconductivity emerges when a Mott insulator with fully localized spins is doped, while already for doping levels $n \sim 0.2$ – 0.25 on a decline of superconductivity, the observed behavior of electronic and magnetic properties is typical for fully itinerant systems. In between these two limits, the observed spin dynamics is characterized by a non-conventional behavior. On the other hand, it is highly believed that Spin Fluctuations (SFs) are at the origin of the high- T_c superconducting pairing in cuprates, see, e.g., Refs. [1–6]. Moreover, it is clear that the spin and charge dynamics are two sides of the same coin in such a strongly correlated system as doped Mott-Neel antiferromagnet (AF). Therefore an understanding of the spin dynamics is a necessary step to achieve a global comprehension of the high- T_c phenomena.

An important progress was made in 2000–2004 when the unusual spin dynamics observed by neutron scattering in the superconducting (SC) state of near-optimally doped cuprates was successfully explained based on the spin-exciton scenario within the fully itinerant electron picture. It was, namely, shown that due to the opening of a SC gap of d symmetry, a resonance mode with a downward dispersion appears below a certain characteristic energy (the so-called resonance energy) ω_r , see Ref. [7]. Since then, new issues have been raised by inelastic neutron experiments (INS) for low and moderate dopings

[21–36]. First, the magnetically ordered incommensurate state was discovered for doping $n < n_c \sim 0.08$ – 0.09 . Second, the observed spin dynamics was found to be qualitatively the same in the normal and SC states—no strong enhancement in crossing T_c when lowering T and no resonance, in contrast to near optimally doped cuprates. The most characteristic features of the observed at low and moderate doping normal-state spin dynamics are the following. The spectrum near \mathbf{Q}_{AF} is characterized by two components having qualitatively different behavior. The component above the characteristic energy ω_c has an upward dispersion, the spin excitations are reminiscent of spin waves in undoped insulating state having however a reduced spectral weight. The component below ω_c is quite narrow in q and has a slight downward dispersion, the spin excitations are anisotropic in the momentum space being incommensurate in one in-plane direction and commensurate in the other. The two components do not cross at \mathbf{Q}_{AF} , as it happens in the SC state for near optimal doping; due to this the dispersion is sometimes called an OPEN-hour-glass shaped. [On the other hand, due to the narrowness in q of the component below ω_c , the dispersion is sometimes also called an Y shaped.] For doping exceeding n_c , the normal-state spin fluctuations keep most of the above described features but acquire a gap. The behavior as a whole is very different from the archetypal behavior of the optimally doped cuprates. It is clear that the mechanism behind such a normal-state spin dynamics is different from the spin-exciton scenario valid for the SC state (and corresponding to the fully itinerant electron picture). On the other hand, the observed behavior, although it appears first in the magnetically ordered incommensurate phase, is very different from the behavior predicted for helicoidal magnets within localized-spin

theories with the cone-shaped dispersion, the resonant character of fluctuations, and the uniform spectral weight.

The results obtained in the present paper seem able to shed light on the origin of the observed nonconventional normal-state spin dynamics. We study on a microscopic level the state with spiral order of localized spins appearing in strongly correlated electron systems that arises upon doping a 2D Neel AF paying special attention to an accurate treatment of kinematic and dynamic interactions between localized spins and mobile charges. We show that this interaction is responsible for many nonconventional features of the spin dynamics in such a spiral state. These features concern the energy-momentum (ω - \mathbf{q}) areas beyond the area of an immediate proximity to the $\omega \rightarrow 0$, $\mathbf{q} \rightarrow \pm \mathbf{Q}_{\text{sp}}$ points where the obtained results are close to those in the previous theories [37–44] (\mathbf{Q}_{sp} is the spiral order wave vector). [Note that in the frequently used to study the spiral state slave-fermion approach [45–51], the spin dynamics was practically not considered. The reason is that in this approach, the physical spins and charges turn out to be two-particle objects, compounds of auxiliary quasiparticles, spinons and holons, which makes their study difficult; it is the problem of stability of the spiral states of different symmetries, the properties of spinons and holons, etc., that were mainly explored within this approach.] Namely, we find that due to the interaction with mobile holes, a characteristic energy emerges above and below which the spin dynamics is qualitatively different. [This energy (we call it ω_c) is proportional to the spiral incommensurability wave vector $Q = |\mathbf{Q}|$ and increases with doping ($\mathbf{Q} \equiv \mathbf{Q}_{\text{AF}} - \mathbf{Q}_{\text{sp}}$, where \mathbf{Q}_{AF} is the AF wave vector)]. Above ω_c , spin excitations have a resonant character typical usually for localized-spin systems, while below it, coherent excitations disappear in the in-plane fluctuation spectrum, and SFs have a relaxation character typical usually for itinerant electron systems. The high-energy magnonlike component having an upward dispersion can be roughly seen as a transformation of the AF-state spin waves, which get a gap due to the incommensurability of the magnetic order and have a reduced spectral weight being accompanied for fixed ω by a continuum of two-particle fluctuations. The component below ω_c reflects an impact of mobile holes on SFs; it has a slight downward dispersion, the spectra are anisotropic being incommensurate in one in-plane direction and commensurate in the other. The low-energy characteristic wave vector of this component is neither the localized-spin spiral wave vector \mathbf{Q} nor the $2\mathbf{k}_F$, as it would be in the metallic SDW state, and is always much smaller than $2k_F$. This is why this component is quite narrow in q . The two components are not crossing at \mathbf{Q}_{AF} but form a sort of a neck around the energy ω_c with the neck width Δq_{neck} proportional to Q . There is no resonance at ω_c . There is no qualitative difference between the behavior in the normal and SC states as far as doping is relatively low. The latter features, the overall form of the dispersion of spin excitations (that can be considered as OPEN-hour-glass shaped since the spin excitations are incommensurate even at ω_c or Y-shaped because of the narrowness of the dispersion below the energy ω_c), the details of their behavior above and below ω_c , and the doping dependencies of the characteristic energy and the characteristic wave vectors are close to those observed experimentally in low-doped cuprates.

The mechanism that is behind such spin dynamics can roughly be understood as follows. Due to the kinematic spin-charge interaction, the spiral order in the localized-spin subsystem induces an off-diagonal order in the itinerant-charge subsystem and a gap in the hole spectrum. This occurs on a level of dynamically noninteracting quasiparticles. Due to the dynamic spin-charge interaction, this gap in the hole spectrum produces a feedback effect consisting in the appearance of a gap in the coherent spin excitation spectrum. The upper branch of this spectrum (above the gap) corresponds to the magnonlike fluctuations mentioned above. The lower branch (below the gap) is what is left of the spiral-state Goldstone mode (mandatory in the long-range ordered state as responsible for the breaking of continuous symmetry)—being truncated by the gap from above, the Goldstone mode survives only in its initial part at very low energies, see comment [52]. Inside the gap, incoherent spin excitations of two-particle electron-hole origin are settled. Further, we find that the long-range-ordered (LRO) spiral state becomes unstable at a certain critical doping n_c . If we adopt a natural hypothesis that the paramagnetic (PM) state above n_c keeps finite-energy spiral correlations and use the obtained in the paper results for the static spiral state, it becomes possible to understand the spin dynamics observed in the so-called pseudogap state as well as the tendencies of the doping evolution of spin excitations in cuprates from low to high doping.

The paper is organized as follows. In Sec. II, we discuss the kinematic interrelation between spin and charge degrees of freedom in the system arising upon doping the insulating Mott-Neel AF and described by the t - J model. It consists in the fact that the Hubbard operators (HOs) describing spin- and charge- degrees of freedom form a common algebra, which is equivalent to the existence of a kinematic spin-charge interaction. In Sec. III, we introduce the representation of these operators in terms of Bose/Fermi operators, which is the extension of the Dyson-Maleev representation for spin operators onto the algebra $Sp(1,2)$ of the eight HOs of the t - J model. It is much better adapted for the study of magnetically ordered systems with broken rotational symmetry than the slave-fermion/slave-boson representations that as the extensions of the Schwinger-boson/Abrikosov-fermion representations are suitable to study states with preserved rotational symmetry. Moreover, it preserves accurately the local constraint between the spin and charge degrees of freedom that is very important if one wishes to treat correctly the spin-charge interrelation. As this representation supposes that the quantization axis points along the magnetization on each site of the lattice, we perform first an unitary transformation to local coordinates which turn in space as the spiral. In Sec. IV, we consider the spin and charge dynamics in the dynamically noninteracting-quasiparticle approximation. The important results for the charge dynamics are the appearance of an off-diagonal order and the opening of a gap in the fermion spectrum as well as a shift of the Fermi pocket centers with respect to the commensurate positions in the Brillouin zone (BZ). As to the spin dynamics, we find a splitting of the spin-wave spectrum with respect to the AF case, with one Goldstone and one optical mode. The behavior of the latter reveals an instability of the spiral state immediately upon doping in the case of isotropic exchange interaction and its stabilization for doping $n < n_c$.

in the presence of a small easy-plane anisotropy $1 - \zeta$; n_c is the doping at which the spiral order incommensurability wave vector reaches its critical value $Q_c = 2\sqrt{1 - \zeta}$. (As known, for cuprates $1 - \zeta$ is relatively high, namely, $1 - \zeta \sim 10^{-3}$ [53–56].) In Sec. V, we study changes in spin dynamics due to the dynamical spin-charge interaction. The Green function formalism allowing to get expressions for the in-plane and out-of-plane spin response functions and SF spectrum through polarization operator components is presented in Sec. V A. In Sec. V B, the polarization operator components are calculated analytically in the low-carrier-density approximation; the analysis of the impact of their structure on renormalized spin fluctuation spectrum is presented as well. In Sec. VI, we apply the formalism to cuprates; Sec. VI A treats the LRO spiral state, while in Sec. VI B, the spin dynamics above the critical doping n_c is discussed. Section VII contains Summary and Discussion.

II. t - J MODEL. INTERRELATION BETWEEN SPIN AND CHARGE DEGREES OF FREEDOM

The t - J model is a good model to describe the system of interrelated localized spins and mobile charges resulting from the doping of the AF Mott-insulator state (t includes nearest neighbors, next-nearest neighbors, etc.). It was introduced first, from the one-band Hubbard model [57,58], and later from the three-band Hubbard model for CuO₂ plane [59–61]. In the latter case, the CuO₂ plane is represented as a lattice of plaquettes centered on copper sites; each plaquette contains a Cu site and four nearest neighbor O sites. The Hamiltonian of the t - J model is written as

$$\begin{aligned} H &= H_t + H_J - \mu \sum_i X_i^{00}, \\ H_t &= \sum_{ij} \sum_{\sigma=1,-1} t_{ij} X_i^{0\sigma} X_j^{\sigma 0}, \\ H_J &= \frac{1}{2} \sum_{(ij)} \sum_{\sigma=1,-1} J_{ij} (X_i^{\sigma\bar{\sigma}} X_j^{\bar{\sigma}\sigma} - X_i^{\sigma\sigma} X_j^{\bar{\sigma}\bar{\sigma}}), \end{aligned} \quad (1)$$

where t_{ij} is a general notation for the terms corresponding to nearest neighbors (nn) (t), next nearest-neighbors (nnn) (t'), and next-next-nearest neighbors (nnnn) (t'') hopping ($t' \neq 0$ and $t'' \neq 0$ reflecting a nonlocal character of the cooper-oxygen singlet state); for the exchange interaction J_{ij} , only the nn terms are present, μ is the chemical potential. The model is formulated in terms of the so-called Hubbard operators (HOs), $X_i^{pq} = |i, p\rangle\langle i, q|$, that describe transitions between $|q\rangle$ and $|p\rangle$ states on the lattice site i . The HOs are defined by their multiplication rules

$$X_i^{pq} X_i^{q'p'} = \delta_{qq'} X_i^{pp'}, \quad (2)$$

the commutation relations

$$[X_i^{pq}, X_j^{q'p'}]_{\pm} = \delta_{ij} (\delta_{qq'} X_i^{pp'} \pm \delta_{pp'} X_i^{q'q}) \quad (3)$$

and the sum rule

$$\sum_p X_i^{pp} = 1, \quad (4)$$

[\pm in (3) stands for the anticommutator and commutator, respectively, the sign “+” corresponds to the case when both

HOs are Fermi-like and the sign “−” does to the case when at least one of them is Bose-like. In the case of the t - J model, there are three one-site states ($p, q = 0, 1, -1$) and therefore eight HOs X_i^{pq} . The states $|1\rangle$ and $|-1\rangle$ correspond to the states of the plaquette with one (localized) hole on copper having spin up and down respectively and the state $|0\rangle$ corresponds to the singlet bound state of two holes on the plaquette (one on oxygen and another on copper). Therefore the two operators X_i^{1-1} , X_i^{-11} describe transitions between the up, down states of localized spin and the four operators $X_i^{\pm 10}$, and $X_i^{0\pm 1}$ describe transitions between the states with zero spin and spin up/down concerning the spin degrees of freedom, and the creation and annihilation of a “hole” concerning the charge degrees of freedom. Correspondingly, the operators $X_i^{\pm 10}$, $X_i^{0\pm 1}$ are Fermi-like [the sign “+” in (3)], while the operators X_i^{1-1} , X_i^{-11} (and all the diagonal operators, X_i^{11} , X_i^{-1-1} , and X_i^{00}) are Bose-like [the sign “−” in (3)]. These eight independent operators X_i^{pq} form a close algebra [Lie superalgebra $Sp(1,2)$] so that the operators describing the “holes” and spins turn out to be interrelated, which is equivalent to a kinematic charge-spin interaction.

Note that since the Bose-like HOs coincide with the spin operators,

$$S^+ = X^{1-1}, \quad S^- = X^{-11}, \quad S^z = \frac{1}{2}(X^{11} - X^{-1-1}), \quad (5)$$

the term H_J in the Hamiltonian (1) can be also written as

$$H_J = \sum_{(ij)} J_{ij} \left(S_i^x S_j^x + S_i^z S_j^z + \zeta S_i^y S_j^y - \frac{1}{4} n_i^e n_j^e \right), \quad (6)$$

($\alpha = x, y, z$, $n_i^e = X_i^{11} + X_i^{-1-1}$ is a number of “electrons” on the site i), from where one sees that at zero doping the Hamiltonian of the t - J model is reduced to the Heisenberg Hamiltonian describing the localized $s = 1/2$ spins on a square lattice. [In Eq. (6), we introduce a small easy plane anisotropy $1 - \zeta > 0$; although the original t - J model (1) is isotropic, $\zeta = 1$, for the cuprates the in-plane anisotropy is relatively high, $1 - \zeta \sim 10^{-3}$ [53–56], on the other hand, its presence is important for the stability of the spiral state, as we will see later on.] Due to the sum rule (4), the total number of “electrons” and “holes” in the t - J model is 1 : $\langle n_i^e \rangle + \langle n_i^h \rangle = 1$ ($n_i^h \equiv X_i^{00}$). The hole density $\langle n_i^h \rangle \equiv n$ is equal to doping.

On the other hand, since the Fermi-like $X_i^{0\sigma}$, $X_i^{\sigma 0}$ operators coincide with the constrained creation and annihilation operators of “hole” with spin σ on the lattice site i ,

$$\tilde{C}_{i\uparrow}^+ = X_i^{01}, \quad \tilde{C}_{i\downarrow}^+ = X_i^{0-1}, \quad (7)$$

the term H_t in the Hamiltonian (1) can be written also as

$$H_t = \sum_{ij} \sum_{\sigma} t_{ij} \tilde{C}_{i\sigma}^+ \tilde{C}_{j\sigma}. \quad (8)$$

III. UNITARY TRANSFORMATION TO LOCAL COORDINATES. EXTENDED DYSON-MALEEV REPRESENTATION

It is difficult to work with the Hubbard operators since their statistics is different from that of Fermi/Bose operators for which methods of theoretical physics are well developed. Different approaches are possible. The first consists of using the

diagrammatic technique for the HOs (see, e.g., Refs. [62–64]) and is rather complex. The second consists of using a representation of the HOs in terms of Bose/Fermi operators. Usually, the results obtained within the second approach are more transparent. (The equation-of-motion approach is also possible, however, the decoupling schemes used in this case are not much controllable.) The known representations are the slave-fermion (SF) [45–51] and the slave-boson (SB) [65–68] representations that are respectively the extensions of the Schwinger-boson and Abrikosov-fermion representations for spin operators onto the algebra $\text{Spl}(1,2)$, the representations [69] and [70] that are respectively the extensions of the Dyson-Maleev (DM) and Holstein-Primakoff (HP) representations for spin operators onto the algebra $\text{Spl}(1,2)$, the “normal Fermi-liquid” representations [64] [Eq. (A4)] and the equivalent representation [71], see Ref. [72]. All of them are not exact in the same manner as the original representations for spin operators. In particular, all of them expand the states of the Hamiltonian by introducing unphysical states.

Use of different representations reduces the initial t - J model to different spin-fermion models corresponding to different limits (see, e.g., an analysis of the different representations in Ref. [64], Appendix A). A choice of representation should be dictated mainly by the proximity of the studied state to the limit to which the representation is most adapted (i.e., in which the population of the unphysical states is small). Note that the Hamiltonian of the t - J model is an extension of the Heisenberg Hamiltonian for $s = 1/2$ localized spins and the Lie superalgebra $\text{Spl}(1,2)$ is an extension of the Lie algebra $\text{SU}(2)$ formed by the spin $1/2$ operators, therefore a relevant representation for HOs of the former algebra should be an extension of the relevant representation for spin $s = 1/2$ operators. As known, in the latter case, there are two types of the representations: DM/HP representations adapted for studying of the ordered states with broken rotational symmetry and the Schwinger-boson/Abrikosov-fermion representations used usually to study states that conserve the rotational symmetry. It is clear that the suitable representation to study physical properties of states with rotationally broken symmetry in our hole doped system, including the states with the spiral order of localized spins, is not an extension of the Schwinger-boson/Abrikosov-fermion representation but that of the DM/HP representation. Such a representation extended to the algebra of the 8 HOs of the t - J model was proposed in Ref. [69] (the DM variant) and in Ref. [70] (the HP variant). This representation supposes that the quantization axis z points along the magnetization on each site of the lattice. Therefore, to be applied to a noncollinear LRO magnetic state, it must be preceded by a unitary transformation to “local coordinates” in which on each lattice site the quantization axis z is parallel to the local magnetization.

We consider the AF coplanar spiral state (in the zx plane) with the angle between the magnetization vectors on nn sites i , $i + \hat{\eta}$ constant through the lattice and equal to $\mathbf{Q}_{\text{AF}} - \phi_{i\hat{\eta}}$ [$\mathbf{Q}_{\text{AF}} = (\pi, \pi)$ is the AF wave vector, $\hat{\eta} = \hat{x}, \hat{z}$, $\phi_{i\hat{\eta}}$ is supposed small]. It is convenient to introduce the local coordinates of the AF type in which on the site i (lattice A) the magnetization points up and on the nn site $i + \hat{\eta}$ (lattice B), it points down with respect to the local quantization axis z . To pass to this local basis we have to rotate through an angle $\phi_i = \mathbf{Q}\mathbf{R}_i$ on each

site, i.e., to apply to the Hamiltonian the unitary transformation $V_\alpha : \tilde{H} = V_\alpha H V_\alpha^{-1}$, $V_\alpha = \exp(i \sum_i \phi_i S_i^\alpha)$. (The wave vector \mathbf{Q} should be determined self-consistently, we will do this in Sec. VI A.)

The explicit form of the transformation of the eight operators X_i^{pq} of the t - J model under such a unitary transformation can be found by using the formalism of the Wigner D matrix. For the three components corresponding to the spin operators, it is the $D^{(1)}$ matrix of the dimension 3 that determines the transformation, while for the other five components, it is the $D^{(2)}$ matrix of the dimension 5 that is involved. In the case of the rotations about the axis y (that we need to perform in our case of zx plane), we get

$$\begin{aligned} X_i^{11} &= \frac{1}{2} [\tilde{X}_i^{11} (1 + \cos \phi) + \tilde{X}_i^{-1-1} (1 - \cos \phi) \\ &\quad - (\tilde{X}_i^{1-1} + \tilde{X}_i^{-11}) \sin \phi], \\ X_i^{-1-1} &= \frac{1}{2} [\tilde{X}_i^{11} (1 - \cos \phi) + \tilde{X}_i^{-1-1} (1 + \cos \phi) \\ &\quad + (\tilde{X}_i^{1-1} + \tilde{X}_i^{-11}) \sin \phi], \\ X_i^{1-1} &= \frac{1}{2} [\tilde{X}_i^{1-1} (1 + \cos \phi) - \tilde{X}_i^{-11} (1 - \cos \phi) \\ &\quad + (\tilde{X}_i^{11} - \tilde{X}_i^{-1-1}) \sin \phi], \\ X_i^{10} &= \tilde{X}_i^{10} \cos \frac{\phi}{2} - \tilde{X}_i^{-10} \sin \frac{\phi}{2}, \\ X_i^{-10} &= \tilde{X}_i^{-10} \cos \frac{\phi}{2} + \tilde{X}_i^{10} \sin \frac{\phi}{2}, \end{aligned} \quad (9)$$

where X_i^{pq} and \tilde{X}_i^{pq} are the HOs in the initial and new basis, respectively. For X_i^{-11} and X_i^{01} X_i^{0-1} , one should use $X_i^{pq} = (X_i^{qp})^\dagger$. In (9), $\phi = \phi_i = \mathbf{Q}\mathbf{R}_i$.

It is clear from (9) that in the new basis the Hamiltonian \tilde{H} contains not only the terms of the same structure as in (1) (with the renormalized interactions, \tilde{t}_{ij} , \tilde{J}_{ij}), but also new terms. Those are $\sum_{ij} R_{ij} \tilde{X}_i^{01} \tilde{X}_j^{-10} + \text{H.c.}$ for the charge degrees of freedom and $\sum_{ij} Q_{ij} \tilde{X}_i^{1-1} \tilde{X}_j^{-1-1} + \text{H.c.}$ for the spin degrees of freedom.

We now introduce boson b and fermion f by using the representation [69]

$$\begin{aligned} \tilde{X}_i^{10} &= f_i, \quad \tilde{X}_i^{01} = f_i^+ (1 - b_i^+ b_i), \\ \tilde{X}_i^{-10} &= b_i^+ f_i, \quad \tilde{X}_i^{0-1} = f_i^+ b_i, \\ \tilde{X}_i^{1-1} &= b_i, \quad \tilde{X}_i^{-11} = b_i^+ (1 - b_i^+ b_i - f_i^+ f_i), \\ \tilde{X}_i^{00} &= f_i^+ f_i, \quad \tilde{X}_i^{-1-1} = b_i^+ b_i, \\ \tilde{X}_i^{11} &= 1 - b_i^+ b_i - f_i^+ f_i, \end{aligned} \quad (10)$$

that is an extension of the Dyson-Maleev representation for $s = 1/2$ to the algebra of eight operators of the t - J model. One can easily check that this representation preserves exactly the commutation relations (3) and the local constraint (4). The matrix elements of transitions between physical and unphysical states are zero. (The physical subspace is obtained by considering the states with $b_i b_i = 0$ and $b_i f_i = 0$.) Therefore, when used for a magnetically ordered state this representation is asymptotically exact in the case of low T and small hole concentration n . [Note the difference with the

SF/SB representation in which the local constraint (4) cannot be fulfilled and is replaced by the enforced global constraint $(1/N) \sum_i (\sum_p X_i^{pp}) = 1$.] Since our local coordinates are of AF type we should use (10) for sublattice A, while for sublattice B, we should replace in Eq. (10) $1 \leftrightarrow -1$ and introduce a - and g operators instead of b and f , respectively.

Performing explicitly all described above transformations, we get the Hamiltonian

$$H = H_s + H_h + H_{s-h}, \quad (11)$$

where H_s contains only Bose operators and describes the spin subsystem, H_h contains only Fermi operators and describes the ‘‘hole’’ subsystem, and H_{s-h} describes the interaction between the two subsystems.

IV. SPIN AND CHARGE DYNAMICS IN NONINTERACTING-QUASIPARTICLE APPROXIMATION

A. Spin dynamics: spectra, magnon and spin Green functions

The magnetic part of the Hamiltonian, H_s , includes a quadratic term $H_s^{(2)}$ describing noninteracting ‘‘magnons’’ and high-order terms $H_s^{(l)}$ ($l = 4$ and 6) describing magnon-magnon scattering, usually small at low T :

$$H_s = E_0^s + H_s^{(2)} + H_s^{(4)} + H_s^{(6)}.$$

The quadratic Hamiltonian and the energy E_0^s are given by

$$\begin{aligned} H_s^{(2)} &= \sum_{\mathbf{q}} [A_{\mathbf{q}}(a_{\mathbf{q}}^+ a_{\mathbf{q}} + b_{\mathbf{q}}^+ b_{\mathbf{q}}) + C_{\mathbf{q}}(a_{\mathbf{q}}^+ b_{-\mathbf{q}}^+ + b_{-\mathbf{q}} a_{\mathbf{q}})] \\ &\quad + D_{\mathbf{q}}(a_{\mathbf{q}} b_{\mathbf{q}}^+ + b_{\mathbf{q}} a_{\mathbf{q}}^+), \\ E_0^s &= -N(J_{\mathbf{Q}} + J_{-\mathbf{Q}})/16, \end{aligned} \quad (12)$$

where

$$\begin{aligned} A_{\mathbf{q}} &= \frac{1}{4}(J_{\mathbf{Q}} + J_{-\mathbf{Q}}), \quad C_{\mathbf{q}} = \frac{1}{4}[\zeta J_{\mathbf{q}} + \frac{1}{2}(J_{\mathbf{q}+\mathbf{Q}} + J_{\mathbf{q}-\mathbf{Q}})], \\ D_{\mathbf{q}} &= -\frac{1}{4}[\zeta J_{\mathbf{q}} - \frac{1}{2}(J_{\mathbf{q}+\mathbf{Q}} + J_{\mathbf{q}-\mathbf{Q}})], \end{aligned} \quad (13)$$

and $J_{\mathbf{q}} = 4J\gamma_{\mathbf{q}}$, $\gamma_{\mathbf{q}} = \frac{1}{2}(\cos q_x + \cos q_z)$. Due to the term with $D_{\mathbf{q}}$, we deal here with a 4×4 dynamic matrix instead of a 2×2 matrix in the case of collinear AF state. Note that for isotropic exchange interaction, i.e., $\zeta = 1$, $D_{\mathbf{q}}$ is zero and the Hamiltonian is reduced to the Hamiltonian of collinear AF if we restrict ourselves by the lowest in Q terms in the full Hamiltonian, i.e., neglect by Q^2 terms in (12), (13) (as can be tempting in the case of low Q). However, it is very important to keep the Q^2 terms, otherwise, we lose the effect of instability of the spiral states in the case of isotropic exchange, i.e., for the standard $t - t' - J$ model, as we will see later on.

The diagonalization of the Hamiltonian (12) is performed applying the following generalized Bogolubov canonical transformation with four eigenvectors:

$$\begin{aligned} a_{\mathbf{q}} &= U_{\mathbf{q}}^+ c_{\mathbf{q}} + V_{\mathbf{q}}^+ c_{-\mathbf{q}}^+ + U_{\mathbf{q}}^- d_{-\mathbf{q}} + V_{\mathbf{q}}^- d_{\mathbf{q}}^+, \\ b_{\mathbf{q}} &= -U_{\mathbf{q}}^+ c_{\mathbf{q}} - V_{\mathbf{q}}^+ c_{-\mathbf{q}}^+ + U_{\mathbf{q}}^- d_{-\mathbf{q}} + V_{\mathbf{q}}^- d_{\mathbf{q}}^+. \end{aligned} \quad (14)$$

After cumbersome but straightforward calculations, we find the following expressions for the eigenvectors and

eigenvalues:

$$(U^{\pm})^2 = \frac{1}{4} \left[\frac{A \mp D}{\Omega^{\pm}} + 1 \right], \quad (V^{\pm})^2 = \frac{1}{4} \left[\frac{A \mp D}{\Omega^{\pm}} - 1 \right],$$

$$U^+ V^+ = \frac{C}{4\Omega^+}, \quad U^- V^- = -\frac{C}{4\Omega^-}, \quad (15)$$

$$(\Omega^{\pm})^2 = (A \mp D)^2 - C^2, \quad (16)$$

while the diagonalized Hamiltonian is written as

$$H_m^{(2)} = \sum_{\mathbf{q}} [\Omega_{\mathbf{q}}^c c_{\mathbf{q}}^+ c_{\mathbf{q}} + \Omega_{\mathbf{q}}^d d_{\mathbf{q}}^+ d_{\mathbf{q}}]. \quad (17)$$

In (17), we renoted the eigenvalues: $\Omega^- \equiv \Omega^d$, $\Omega^+ \equiv \Omega^c$; they describe the dispersions of two branches of the boson spectrum and are given explicitly by

$$\begin{aligned} \Omega_{\mathbf{q}}^d &= \frac{1}{2} \sqrt{(J_{\mathbf{Q}} - \zeta J_{\mathbf{q}}) [J_{\mathbf{Q}} + \frac{1}{2}(J_{\mathbf{q}+\mathbf{Q}} + J_{\mathbf{q}-\mathbf{Q}})]}, \\ \Omega_{\mathbf{q}}^c &= \frac{1}{2} \sqrt{(J_{\mathbf{Q}} + \zeta J_{\mathbf{q}}) [J_{\mathbf{Q}} - \frac{1}{2}(J_{\mathbf{q}+\mathbf{Q}} + J_{\mathbf{q}-\mathbf{Q}})]}. \end{aligned} \quad (18)$$

Note the difference with the AF state, namely a leave of degeneracy between the two branches even in the isotropic case $\zeta = 1$.

Near the AF wave vector, i.e., for $q' \ll 1$ (where $q' = |\mathbf{q}'|$ and $\mathbf{q}' = \mathbf{Q}_{\text{AF}} - \mathbf{q}$), the mode Ω^d is a Goldstone mode with linear dispersion, while the mode Ω^c has a gap, and one can write approximately

$$\begin{aligned} \Omega_{\mathbf{q}}^d &= cq', \quad c = \frac{1}{4} J_0 \sqrt{1 + \zeta}, \\ \Omega_{\mathbf{q}}^c &= \frac{J_0}{2} \sqrt{(\bar{\Delta}^c)^2 + \frac{q'^2}{2}}, \quad \bar{\Delta}^c = \sqrt{2} \sqrt{1 - \zeta - Q^2/4} \end{aligned} \quad (19)$$

($Q = |\mathbf{Q}|$, here and everywhere below we suppose $1 - \zeta \ll 1$). We see that if $\zeta = 1$, then $(\Omega_{\mathbf{q}}^c)^2$ is negative for $q' < Q$, that indicates an instability. Therefore the first conclusion is the following: the coplanar LRO spiral state is unstable in the case of isotropic exchange, i.e., for the standard t - J model. As we will see below, the instability concerns the out-of-plane susceptibility, see Ref. [73]. A presence of a small easy plane anisotropy is enough to stabilize such a state as far as the spiral order incommensurability wave vector is small, namely, as

$$Q < Q_c = 2\sqrt{1 - \zeta}. \quad (20)$$

Note that if we were neglected the terms proportional to Q^2 in the Hamiltonian (12), we would remain with degenerated modes Ω^d and Ω^c and miss the effect of the instability [44].

Near the BZ center, i.e., for $q = |\mathbf{q}| \ll 1$, it is the Ω^d mode that is optical and the Ω^c mode that is a Goldstone mode with linear dispersion, $\Omega_{\mathbf{q}}^c = cq$. For ‘‘high’’ q , $q', q \gg \sqrt{2}\bar{\Delta}^c$, $q' \gg \sqrt{2}\bar{\Delta}^c$, the two modes are practically degenerated, $\Omega_{\mathbf{q}}^c \approx \Omega_{\mathbf{q}}^d$.

Since the Hamiltonian is diagonal on c and d operators, only the diagonal Green functions

$$\begin{aligned} G_{dd^+}(\mathbf{q}, i\omega_n) &\equiv \langle\langle d_{\mathbf{q}} | d_{\mathbf{q}}^+ \rangle\rangle_{i\omega_n} \\ &= - \int_0^{\beta} d\tau e^{i\omega_n \tau} \langle T_{\tau} d_{\mathbf{q}}(\tau) d_{\mathbf{q}}^+(0) \rangle, \\ G_{c^+c}(\mathbf{q}, i\omega_n) &\equiv \langle\langle c_{-\mathbf{q}}^+ | c_{-\mathbf{q}} \rangle\rangle_{i\omega_n} \\ &= - \int_0^{\beta} d\tau e^{i\omega_n \tau} \langle T_{\tau} c_{-\mathbf{q}}^+(\tau) c_{-\mathbf{q}}(0) \rangle \end{aligned} \quad (21)$$

are nonzero, they are equal to

$$\begin{aligned} G_{dd^+}(\mathbf{q}, i\omega_n) &= \frac{1}{i\omega_n - \Omega_{\mathbf{q}}^d}, \\ G_{c+c}(\mathbf{q}, i\omega_n) &= \frac{1}{-i\omega_n - \Omega_{\mathbf{q}}^c}. \end{aligned} \quad (22)$$

In (21) and (22), G_{dd^+} and G_{c+c} are Matsubara Green functions, T_τ is a chronological operator, $\omega_n = 2n\pi T$ are Matsubara discrete frequencies for bosons and τ is the imaginary time. The Green functions determined on the initial a and b operators, that we will need for the following calculations, can be easily obtained from (22) by using Eq. (14).

Those were boson Green functions. Let us now calculate physical spin Green functions, namely the two transversal functions, the out-of-plane one determined as

$$\begin{aligned} G_s^{yy}(\mathbf{q}, i\omega_n) &\equiv \langle\langle S_{\mathbf{q}}^y | S_{\mathbf{q}}^y \rangle\rangle_{i\omega_n} \\ &= - \int_0^\beta d\tau e^{i\omega_n \tau} \langle T_\tau S_{\mathbf{q}}^y(\tau) S_{\mathbf{q}}^y(0) \rangle, \end{aligned} \quad (23)$$

and the in-plane one determined as

$$\begin{aligned} G_s^{xx}(\mathbf{q}, i\omega_n) &\equiv \langle\langle S_{\mathbf{q}}^x | S_{\mathbf{q}}^x \rangle\rangle_{i\omega_n} \\ &= - \int_0^\beta d\tau e^{i\omega_n \tau} \langle T_\tau S_{\mathbf{q}}^x(\tau) S_{\mathbf{q}}^x(0) \rangle. \end{aligned} \quad (24)$$

For this we should use the relation (5) between the spin and Hubbard operators, the transformation (9) from the initial to local coordinates and finally the representation (10) for the HOs through Bose/Fermi operators. Cumbersome but straightforward calculations give

$$\begin{aligned} G_s^{yy}(\mathbf{q}, i\omega_n) &= F_{\mathbf{q}}^c \frac{\Omega_{\mathbf{q}}^c}{(i\omega_n)^2 - (\Omega_{\mathbf{q}}^c)^2}, \\ G_s^{xx}(\mathbf{q}, i\omega_n) &= \frac{1}{2} \left[F_{\mathbf{q}+\mathbf{Q}}^d \frac{\Omega_{\mathbf{q}+\mathbf{Q}}^d}{(i\omega_n)^2 - (\Omega_{\mathbf{q}+\mathbf{Q}}^d)^2} \right. \\ &\quad \left. + (\mathbf{Q} \rightarrow -\mathbf{Q}) \right] + Q^2 O_{\mathbf{q}}, \end{aligned} \quad (25), (26)$$

The prefactors $F_{\mathbf{q}}^c$ and $F_{\mathbf{q}}^d$ in the one-particle terms of (25), (26) are determined as $F_{\mathbf{q}}^c = (U_{\mathbf{q}}^+ - V_{\mathbf{q}}^+)^2$, $F_{\mathbf{q}}^d = (U_{\mathbf{q}}^- + V_{\mathbf{q}}^-)^2$; their explicit dependencies on wave vectors near the AF wave vector (small q') are given by

$$F_{\mathbf{q}}^d = \sqrt{\frac{1+\zeta}{2}} \frac{1}{q'}, \quad F_{\mathbf{q}}^c = \frac{1}{\sqrt{2}} \frac{1}{\sqrt{\Delta_c^2 + q'^2/2}}. \quad (27)$$

The term $Q^2 O_{\mathbf{q}}$ in Eq. (26) corresponds to a higher-order ‘‘many-particle’’ contribution, it is small with respect to the one-particle contribution.

We see that the in-plane Green function (and therefore the in-plane spin susceptibility) contains only the Ω^d mode, while the out-of-plane susceptibility contains only the Ω^c mode. We see also that the out-of-plane Green function is commensurate, while the in-plane spin Green function gets $\mathbf{q} + \mathbf{Q}$, $\mathbf{q} - \mathbf{Q}$ as arguments and therefore is incommensurate. The presence in the in-plane Green function (and in the corresponding susceptibility) of the Goldstone modes at $\mathbf{q}' = \pm\mathbf{Q}$ is related

to the spontaneous breaking in the LRO state of the continuous symmetry of the Hamiltonian (6) corresponding to the rotation around the y axis. Since it is a single continuous symmetry of the Hamiltonian in the case $\zeta \neq 1$, there is no Goldstone mode in the out-of-plane susceptibility.

Note that the gap Δ^c in the optical mode decreases with increasing Q , i.e., with increasing doping (since $Q \propto n$, as we will see in Sec. VI), and vanishes at certain doping $n = n_c$ at which $Q = Q_c$. Therefore the out-of-plane susceptibility χ^{yy} turns out to be a critical susceptibility with respect to the instability at this doping.

The higher-order terms of H_s have a little influence on spin dynamics since the occupation number of the excited states is small at low T . In particular, the magnon-magnon interaction alone does not lead to a finite magnon lifetime at $T = 0$ because the requirement of energy- and momentum-conservation forbids a spontaneous decay of one ‘‘magnon’’ into several magnons. On the contrary, a decay of the ‘‘magnon’’ into two quasiparticles (boson and fermion) occurs due to the spin-hole interaction H_{s-h} that finally strongly modifies the spin dynamics, as we will see in Secs. V and VI. Before to study the role of this interaction let us first analyze the charge dynamics.

B. Charge dynamics: fermionic quasiparticle spectra, charge Green functions

The quadratic on Fermi operators Hamiltonian is given by

$$H_h^{(2)} = (H_h^{(2)})^{(AF)} + \Delta H_h. \quad (28)$$

The first term in (28) is the same as for the collinear AF state [69]

$$(H_h^{(2)})^{(AF)} = \sum_{\mathbf{k}} (\epsilon_{\mathbf{k}} - \mu) (f_{\mathbf{k}}^+ f_{\mathbf{k}} + g_{\mathbf{k}}^+ g_{\mathbf{k}}) \quad (29)$$

with the hole dispersion $\epsilon_{\mathbf{k}}$ having the form

$$\epsilon_{\mathbf{k}} = \epsilon_0 + x_1 (\cos k_x + \cos k_z)^2 + x_2 (\cos 2k_x + \cos 2k_z), \quad (30)$$

where $x_1 = 2t'$ and $x_2 = 2t'' - t'$ (we have neglected unimportant (for the fermions) terms proportional to \mathbf{Q}^2). The location of the minimum of $\epsilon_{\mathbf{k}}$ depends on the relation between t' and t'' , it can be at $(\pi/2, \pi/2)$ or $(0, \pi)$ (in the first quadrant of the BZ). It is well known, however, that the ‘‘dressed’’ holes on the AF background have the dispersion (30) with renormalized parameters x_1 and x_2 such that the minimum of $\epsilon_{\mathbf{k}}$ occurs at $(\pi/2, \pi/2)$ (even when $t' = t'' = 0$), see Refs. [74–80]. The isoenergetical surfaces in this case are given by four ellipses centered at $(\pm\pi/2, \pm\pi/2)$ and having their axes turned by the angle $\pi/4$ with respect to the basic vectors of the reciprocal lattice. In the vicinities of the minima, the dispersion is parabolic,

$$\epsilon_{\mathbf{p}} = ap_{x(y)}^2 + bp_{y(x)}^2, \quad (31)$$

p_x, p_y are the projections of the vector \mathbf{p} on the principal axes of ellipses and $a = 2(x_1 + x_2)$, $b = 2x_2$.

The second term in (28), absent in the collinear AF state, has the form

$$\begin{aligned} \Delta H_h &= \sum_{\mathbf{k}} [B_{\mathbf{k}} (f_{\mathbf{k}}^+ g_{\mathbf{k}} - g_{\mathbf{k}}^+ f_{\mathbf{k}})], \\ B_{\mathbf{k}} &= (t_{\mathbf{k}-\mathbf{Q}/2} - t_{\mathbf{k}+\mathbf{Q}/2})/2i, \end{aligned} \quad (32)$$

where $t_{\mathbf{k}} = 4t\gamma_{\mathbf{k}}$. $B_{\mathbf{k}}$ can be rewritten as

$$B_{\mathbf{k}} = -i2t[\sin(Q_x/2)\sin k_x + \sin(Q_z/2)\sin k_z], \quad (33)$$

where k_α and Q_α are defined in the basic reciprocal space corresponding to the square lattice.

For the matrix fermion Green function in the Matsubara representation

$$\hat{K}(\mathbf{k}, i\omega_n) = -\int_0^\beta d\tau e^{i\omega_n\tau} \langle T_\tau \Phi_{\mathbf{k}}(\tau) \Phi_{\mathbf{k}}^\dagger(0) \rangle, \quad (34)$$

determined on the vector operators Φ and Φ^\dagger ,

$$\Phi = \begin{bmatrix} g_{\mathbf{k}} \\ f_{\mathbf{k}} \end{bmatrix}, \quad \Phi^\dagger = (g_{\mathbf{k}}^\dagger, f_{\mathbf{k}}^\dagger), \quad (35)$$

one gets

$$\hat{K}^{-1}(\mathbf{k}, i\omega_n) = \begin{bmatrix} i\omega_n - \epsilon_{\mathbf{k}} & B_{\mathbf{k}} \\ B_{\mathbf{k}}^* & i\omega_n - \epsilon_{\mathbf{k}} \end{bmatrix}, \quad (36)$$

where $\omega_n = (2n+1)\pi T$ are the Matsubara discrete frequencies for fermions. By inverting (36), we get for the fermion matrix Green-function components the following expressions:

$$\begin{aligned} K_{11}(\mathbf{k}, i\omega_n) &\equiv \langle \langle g_{\mathbf{k}} | g_{\mathbf{k}}^\dagger \rangle \rangle_{i\omega_n} \\ &= \frac{1}{2} \left(\frac{1}{i\omega_n - E_{\mathbf{k}}^+} + \frac{1}{i\omega_n - E_{\mathbf{k}}^-} \right), \\ K_{22}(\mathbf{k}, i\omega_n) &\equiv \langle \langle f_{\mathbf{k}} | f_{\mathbf{k}}^\dagger \rangle \rangle_{i\omega_n} = K_{11}(\mathbf{k}, i\omega_n), \\ K_{12}(\mathbf{k}, i\omega_n) &\equiv \langle \langle g_{\mathbf{k}} | f_{\mathbf{k}}^\dagger \rangle \rangle_{i\omega_n} \\ &= \frac{1}{2} \frac{B_{\mathbf{k}}}{|B_{\mathbf{k}}|} \left(\frac{1}{i\omega_n - E_{\mathbf{k}}^-} - \frac{1}{i\omega_n - E_{\mathbf{k}}^+} \right), \\ K_{21}(\mathbf{k}, i\omega_n) &\equiv \langle \langle f_{\mathbf{k}} | g_{\mathbf{k}}^\dagger \rangle \rangle_{i\omega_n} \\ &= \frac{1}{2} \frac{B_{\mathbf{k}}^*}{|B_{\mathbf{k}}|} \left(\frac{1}{i\omega_n - E_{\mathbf{k}}^-} - \frac{1}{i\omega_n - E_{\mathbf{k}}^+} \right), \end{aligned} \quad (37)$$

where

$$E_{\mathbf{k}}^\pm = \epsilon_{\mathbf{k}} - \mu \pm |B_{\mathbf{k}}| \quad (38)$$

describe the two branches in the fermion spectrum (μ is the chemical potential equal to the Fermi energy $\epsilon_F = \pi n \sqrt{ab}$). We see that in the spiral state the fermion spectrum is split by the gap $\Delta_{\mathbf{k}} = 2|B_{\mathbf{k}}|$. The momentum dependence of the gap is given by Eq. (33). For the (1,1) spiral state ($Q_x = Q_z = Q$), $B_{\mathbf{k}}$ is zero for \mathbf{k} in the (1, -1) direction so that the spectrum near $(-\pi/2, \pi/2)$ and $(\pi/2, -\pi/2)$ remains practically unchanged with respect to the collinear AF state, and the minima are not the absolute minima. In the direction (1,1), $|B_{\mathbf{k}}|$ is maximum at $(\pi/2, \pi/2)$ and $(-\pi/2, -\pi/2)$ so that the latter are the points of absolute minima. For the (1,0) spiral ($Q_x = Q$, $Q_z = 0$), the spectrum has the same minima for the four pockets around $(\pm\pi/2, \pm\pi/2)$.

The calculated above Green functions are the fermion Green functions. Let us calculate now the Green functions describing the physical charges:

$$\begin{aligned} G_h^\sigma(\mathbf{k}, i\omega_n) &\equiv \langle \langle \tilde{C}_{\mathbf{k}\sigma} | \tilde{C}_{\mathbf{k}\sigma}^\dagger \rangle \rangle_{i\omega_n} \\ &= -\int_0^\beta d\tau e^{i\omega_n\tau} \langle T_\tau X_{\mathbf{k}}^{\sigma 0}(\tau) X_{\mathbf{k}}^{0\sigma}(0) \rangle \end{aligned} \quad (39)$$

($\sigma = 1, -1$). By expressing $X^{\sigma 0}$ and $X^{0\sigma}$ operators through the operators \tilde{X}^{pq} in the local coordinates via Eq. (9) and then using the representation (10) for sublattice A and a similar representation for sublattice B, we get

$$\begin{aligned} G_h^\dagger(\mathbf{k}, i\omega_n) &= \frac{1}{2} \left[K_{11} \left(\mathbf{k} + \frac{\mathbf{Q}}{2}, i\omega_n \right) + \frac{1}{i} K_{12} \left(\mathbf{k} + \frac{\mathbf{Q}}{2}, i\omega_n \right) \right] \\ &\quad + \frac{1}{2} \left[K_{11} \left(\mathbf{k} - \frac{\mathbf{Q}}{2}, i\omega_n \right) - \frac{1}{i} K_{12} \left(\mathbf{k} - \frac{\mathbf{Q}}{2}, i\omega_n \right) \right]. \end{aligned} \quad (40)$$

[In (40), we keep only the leading one-particle contributions.] The explicit expression depends on the symmetry of the spiral state and for the chosen symmetry—on the Fermi pocket considered. For both (1,0) and (1,1) spirals, we have near $(\pi/2, \pi/2)$ and $(-\pi/2, -\pi/2)$:

$$G_h^\dagger(\mathbf{k}, i\omega_n) = \frac{1}{2} \left(\frac{1}{i\omega_n - E_{\mathbf{k}+\frac{\mathbf{Q}}{2}}^+} + \frac{1}{i\omega_n - E_{\mathbf{k}-\frac{\mathbf{Q}}{2}}^-} \right) \quad (41)$$

and

$$G_h^\dagger(\mathbf{k}, i\omega_n) = \frac{1}{2} \left(\frac{1}{i\omega_n - E_{\mathbf{k}+\frac{\mathbf{Q}}{2}}^-} + \frac{1}{i\omega_n - E_{\mathbf{k}-\frac{\mathbf{Q}}{2}}^+} \right), \quad (42)$$

respectively. Near $(\pi/2, -\pi/2)$ and $(-\pi/2, \pi/2)$, we have for the (1,0) spiral the expression (41) and (42), respectively, while for the (1,1) spiral we have the expression with a practically nonperturbed spectrum:

$$G_h^\dagger(\mathbf{k}, i\omega_n) \approx \frac{1}{2} \left(\frac{1}{i\omega_n - \epsilon_{\mathbf{k}+\frac{\mathbf{Q}}{2}}} + \frac{1}{i\omega_n - \epsilon_{\mathbf{k}-\frac{\mathbf{Q}}{2}}} \right). \quad (43)$$

For the charge Green function with spin down, $G_h^\downarrow(\mathbf{k}, i\omega_n)$, one should replace $g \leftrightarrow f$ and therefore $i \rightarrow -i$ in (40) that gives for \mathbf{k} in a vicinity of $(\pi/2, \pi/2)$ the same expression as for $G_h^\dagger(\mathbf{k}, i\omega_n)$ for \mathbf{k} in a vicinity of $(-\pi/2, -\pi/2)$ and so on, so that the charge spectra are polarized. For the Green function that includes both polarizations [usually measured by the angle-resolved photoemission (ARPES)], one has near $(\pi/2, \pi/2)$ and $(-\pi/2, -\pi/2)$,

$$\begin{aligned} \sum_\sigma G_h^\sigma(\mathbf{k}, i\omega_n) &= \frac{1}{2} \left[\frac{1}{i\omega_n - E^+(\mathbf{k} + \frac{\mathbf{Q}}{2})} \right. \\ &\quad \left. + \frac{1}{i\omega_n - E^-(\mathbf{k} + \frac{\mathbf{Q}}{2})} + (\mathbf{Q} \rightarrow -\mathbf{Q}) \right], \end{aligned} \quad (44)$$

and the evident expressions for \mathbf{k} in the two other quadrants of the BZ.

Note the important difference between the physical charge Green functions G_h^σ and the fermion Green functions $\langle \langle f_{\mathbf{k}} | f_{\mathbf{k}}^\dagger \rangle \rangle$, $\langle \langle g_{\mathbf{k}} | g_{\mathbf{k}}^\dagger \rangle \rangle$. The former has the same spectrum as the latter, displaced, however, by the vectors $\pm\mathbf{Q}/2$. In other words, the Fermi pocket centers for the physical charges are located not at $(\pm\pi/2, \pm\pi/2)$ but are shifted by half the spiral incommensurability wave vector, as shown in Fig. 1(a) for the (1,1) spiral symmetry and Fig. 1(b) for the (1,0) spiral symmetry. In real crystals, domains of both (1,0) and

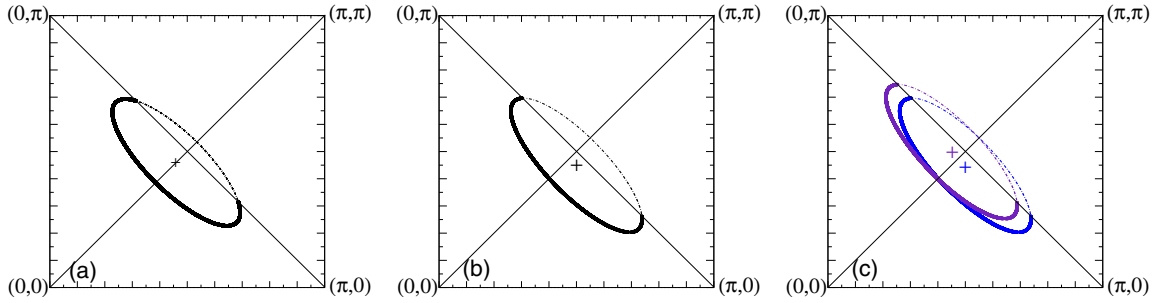


FIG. 1. Schematic plot of the hole Fermi pockets in the first quadrant of BZ: (a) for the (1, 1) spiral state, (b) for the (0, 1) spiral state, (c) for real crystals in which domains of the (0, 1)- and (1, 0)-spiral symmetries can be present simultaneously. The crosses show the centers of the pockets. We present for simplicity the case when only the pockets related to the E^- branch are filled. Note the asymmetry of the pockets with respect to AF BZ boundary.

(0, 1) symmetries can exist simultaneously so that in ARPES experiments, the two corresponding Fermi pockets with the centers displayed by $(Q/2, 0)$ and $(0, Q/2)$ with respect to $(\pi/2, \pi/2)$ could be seen simultaneously, as shown in Fig. 1(c). Note that asymmetric with respect to the AF boundary pockets whose centers are shifted from the commensurate positions were observed in certain ARPES experiments in the normal state of underdoped cuprates [81,82].

C. Off-diagonal charge order

Another important effect in the charge subsystem is the appearance of an off-diagonal order induced by the spiral order of localized spins. The effect is due to the kinematic spin-charge interaction. Indeed, let us consider the charge Green function nondiagonal in spin $\langle\langle \tilde{C}_{\mathbf{k}\sigma} | \tilde{C}_{\mathbf{k}\sigma'}^+ \rangle\rangle$. This Green function being expressed in terms of the fermion Green functions, is given by

$$\begin{aligned} & \langle\langle \tilde{C}_{\mathbf{k}\uparrow} | \tilde{C}_{\mathbf{k}\downarrow}^+ \rangle\rangle_{i\omega_n} \\ &= \frac{1}{2i} \left[-K_{11} \left(\mathbf{k} - \frac{\mathbf{Q}}{2}, i\omega_n \right) + \frac{1}{i} K_{12} \left(\mathbf{k} - \frac{\mathbf{Q}}{2}, i\omega_n \right) \right] \\ & \quad + \frac{1}{2i} \left[K_{11} \left(\mathbf{k} + \frac{\mathbf{Q}}{2}, i\omega_n \right) + \frac{1}{i} K_{12} \left(\mathbf{k} + \frac{\mathbf{Q}}{2}, i\omega_n \right) \right] \end{aligned} \quad (45)$$

(we performed the same transformations as before when calculating the diagonal charge Green function). One can rewrite explicitly, for example, near $(\pi/2, \pi/2)$:

$$\begin{aligned} & \langle\langle \tilde{C}_{\mathbf{k}\uparrow} | \tilde{C}_{\mathbf{k}\downarrow}^+ \rangle\rangle_{i\omega_n} \\ &= \frac{1}{2i} \left[\frac{1}{i\omega_n - E_{\mathbf{k}+\frac{\mathbf{Q}}{2}}^+} - \frac{1}{i\omega_n - E_{\mathbf{k}-\frac{\mathbf{Q}}{2}}^-} \right] \\ &= \frac{1}{i} \frac{|B_{\mathbf{k}+\mathbf{Q}/2}| + |B_{\mathbf{k}-\mathbf{Q}/2}|}{\left[i\omega_n - E_{\mathbf{k}+\frac{\mathbf{Q}}{2}}^+ \right] \left[i\omega_n - E_{\mathbf{k}-\frac{\mathbf{Q}}{2}}^- \right]} \end{aligned} \quad (46)$$

from where we see that the order parameter (OP) $\phi_{\mathbf{k}} = \langle\langle \tilde{C}_{\mathbf{k}\uparrow}^+(t) \tilde{C}_{\mathbf{k}\downarrow}(t) \rangle\rangle$ is proportional to Q ,

$$\phi_{\mathbf{k}} \propto |B_{\mathbf{k}=(\pi/2, \pi/2)}| \propto Q. \quad (47)$$

The OP is obtained by using the Green-function-formalism theorem that relates an average of operators to the correspond-

ing Green function:

$$\langle B(t') A(t) \rangle = \int_{-\infty}^{\infty} d\omega n^F(\omega) \rho_{AB}(\omega) e^{-i\omega(t-t')},$$

where $\rho_{AB} = G_{AB}^r(\omega + i\delta) - G_{AB}^r(\omega - i\delta)$ is the spectral function and G^r is the Green function in retarded representation. The OP $\phi_{\mathbf{k}}$ describes the off-diagonal order in the charge subsystem, which corresponds to Bose condensation of electron-hole pairs with total spin zero—the pairing similar to the singlet SC pairing but concerning an electron and a hole instead of two electrons (i.e., of DW nature). In Ref. [83], we show that such an order also appears in the case when spiral correlations of localized spins are short-range and that it has a certain relation to the so-called intra unit cell $\mathbf{q} = 0$ magnetic order observed in cuprates in the pseudogap phase [84]. We discuss this in details in Ref. [83]. Here it is important to emphasize that the appearance of this off-diagonal charge order is a direct consequence of the spin-charge kinematic interaction, which consists in the fact that the spin and charge Hubbard operators form a common algebra and therefore the charge HOs (and thus the charge degrees of freedom) are also affected by the unitary transformation to the local coordinates concerning the spin subsystem and they feel in this way the incommensurability of the localized spin order. This is one of the manifestation of strong-electron-correlation aspect in the considered approach.

V. THE EFFECT OF THE DYNAMIC SPIN-CHARGE INTERACTION ON THE SPIN DYNAMICS

Let us now study effects of the dynamic spin-charge interaction on spin dynamics. The most important term of such an interaction is given by the Hamiltonian of third order

$$\begin{aligned} H_{s-h}^{(3)} = & \sum_{\mathbf{k}, \mathbf{q}} \left[t_{\mathbf{k}+\frac{\mathbf{Q}}{2}} g_{\mathbf{k}}^+ f_{\mathbf{k}+\mathbf{q}} b_{\mathbf{q}}^+ \right. \\ & \left. + t_{\mathbf{k}+\mathbf{q}+\frac{\mathbf{Q}}{2}} g_{\mathbf{k}}^+ f_{\mathbf{k}+\mathbf{q}} a_{-\mathbf{q}} + (Q \rightarrow -Q) \right] \end{aligned} \quad (48)$$

describing a decay of Bose quasiparticle, magnon, into two Fermi quasiparticles, “electron” and “hole.” Note that this process turns out to be associated with the highest energetical parameter (t) in the $t-t'-J$ model.

A. Renormalised “magnon” and spin Green functions

First we rewrite $H_{s-h}^{(3)}$ in terms of c and d operators. Two independent groups of terms emerge: the first is coming from the U^- and V^- coefficients and the d operators, i.e., from the d mode, and the second is coming from the U^+ and V^+ coefficients and the c operators, i.e., from the c mode:

$$\begin{aligned} H_{s-h}^{(3)} &= H_d^{(3)} + H_c^{(3)}, \\ H_d^{(3)} &= t_0 \sum_{\mathbf{k}, \mathbf{q}} (M_{\mathbf{k}-\mathbf{q}, \mathbf{q}}^d g_{\mathbf{k}}^+ f_{\mathbf{k}-\mathbf{q}} d_{-\mathbf{q}} + \text{H.c.}), \\ H_c^{(3)} &= t_0 \sum_{\mathbf{k}, \mathbf{q}} (M_{\mathbf{k}-\mathbf{q}, \mathbf{q}}^c g_{\mathbf{k}}^+ f_{\mathbf{k}-\mathbf{q}} c_{\mathbf{q}} + \text{H.c.}), \end{aligned} \quad (49)$$

with the scattering amplitudes given by

$$\begin{aligned} M_{\mathbf{k}-\mathbf{q}, \mathbf{q}}^d &= \frac{1}{2} [U_{\mathbf{q}}^- \gamma_{\mathbf{k}-\mathbf{q}+\frac{\mathbf{q}}{2}} + V_{\mathbf{q}}^- \gamma_{\mathbf{k}+\frac{\mathbf{q}}{2}} + (Q \rightarrow -Q)], \\ M_{\mathbf{k}-\mathbf{q}, \mathbf{q}}^c &= \frac{1}{2} [U_{\mathbf{q}}^+ \gamma_{\mathbf{k}-\mathbf{q}+\frac{\mathbf{q}}{2}} - V_{\mathbf{q}}^+ \gamma_{\mathbf{k}+\frac{\mathbf{q}}{2}} + (Q \rightarrow -Q)]. \end{aligned} \quad (50)$$

The latter can be rewritten in a more symmetrical form:

$$\begin{aligned} M_{\mathbf{k}-\mathbf{q}, \mathbf{q}}^d &= \frac{1}{4} [(U_{\mathbf{q}}^- + V_{\mathbf{q}}^-)(\gamma_{\mathbf{k}-\mathbf{q}+\frac{\mathbf{q}}{2}} + \gamma_{\mathbf{k}+\frac{\mathbf{q}}{2}}) \\ &\quad + (U_{\mathbf{q}}^- - V_{\mathbf{q}}^-)(\gamma_{\mathbf{k}-\mathbf{q}+\frac{\mathbf{q}}{2}} - \gamma_{\mathbf{k}+\frac{\mathbf{q}}{2}}) + (Q \rightarrow -Q)], \\ M_{\mathbf{k}-\mathbf{q}, \mathbf{q}}^c &= \frac{1}{4} [(U_{\mathbf{q}}^+ - V_{\mathbf{q}}^+)(\gamma_{\mathbf{k}-\mathbf{q}+\frac{\mathbf{q}}{2}} + \gamma_{\mathbf{k}+\frac{\mathbf{q}}{2}}) \\ &\quad + (U_{\mathbf{q}}^+ + V_{\mathbf{q}}^+)(\gamma_{\mathbf{k}-\mathbf{q}+\frac{\mathbf{q}}{2}} - \gamma_{\mathbf{k}+\frac{\mathbf{q}}{2}}) + (Q \rightarrow -Q)] \end{aligned} \quad (51)$$

from which we see that $M^d \rightarrow 0$ when $q \rightarrow \mathbf{Q}_{\text{AF}}$ ($q' \rightarrow 0$), i.e., in the region where Ω^d is a Goldstone mode, and $M^c \rightarrow 0$ when $q \rightarrow 0$, i.e., in the region near the BZ center where Ω^c is a Goldstone mode, as it should be in a correspondence to the Adler theorem for scattering amplitudes. More precisely, $(M^d)^2 \propto q'$ when $q' \rightarrow 0$, and $(M^c)^2 \propto q$ when $q \rightarrow 0$. Below we will consider spin fluctuations near the AF wave vector.

As usual in the case of quasiparticles with strong interaction (here t) but small quasiparticle density (here density of the doped holes n), the actual expansion parameter is proportional to the density and is equal here to $(t/J)n$. This is why for small n one can take into account only the lowest-order graphs, which for the interaction (49) are the bubble graphs. (The approximation is very good due to the absence of single loop corrections in the spin-charge vertex, the reason is the same as for AF state, see Refs. [75,76].) The Hamiltonian (49) does not conserve the number of “magnons” and therefore the spin-charge interaction induces not only a renormalization of the diagonal Green functions G_{c+c} and G_{dd} but also an appearance of off-diagonal components. Then, for renormalized magnon Green functions, we should introduce the matrix

$$\hat{G}(\mathbf{q}, i\omega_n) = - \int_0^\beta d\tau e^{i\omega_n \tau} \{T_\tau \Psi_{\mathbf{q}}(\tau) \Psi_{\mathbf{q}}^\dagger(0)\} \quad (52)$$

defined on vector operators

$$\Psi = \begin{bmatrix} d_{\mathbf{q}} \\ d_{\mathbf{q}}^+ \\ c_{-\mathbf{q}}^+ \\ c_{\mathbf{q}} \end{bmatrix}, \quad \Psi^\dagger = (d_{\mathbf{q}}^+, d_{-\mathbf{q}}, c_{-\mathbf{q}}, c_{\mathbf{q}}^+). \quad (53)$$

Straightforward calculations show that the result of summation of infinite series of different bubble graphs can be presented as a matrix Dyson equation $\hat{G}^{-1} = (\hat{G})^{-1} - \hat{\Pi}$ written explicitly as

$$\hat{G}^{-1} = - \begin{bmatrix} A^d - i\omega_n & D^d & B & C \\ D^d & A^d + i\omega_n & C & B \\ B & C & A^c + i\omega_n & D^c \\ C & B & D^c & A^c - i\omega_n \end{bmatrix}. \quad (54)$$

In (54), $A^d = \Omega_{\mathbf{q}}^d + \Pi_d^+(\mathbf{q}, i\omega_n)$, $A^c = \Omega_{\mathbf{q}}^c + \Pi_c^+(\mathbf{q}, i\omega_n)$, $D^d = -\Pi_d^-(\mathbf{q}, i\omega_n)$, $D^c = -\Pi_c^-(\mathbf{q}, i\omega_n)$, $B = -\Pi_{cd}^+(\mathbf{q}, i\omega_n)$, $C = \Pi_{cd}^-(\mathbf{q}, i\omega_n)$, and $\Pi_{c,d}^\pm$ are the components of the matrix polarization operator $\hat{\Pi}$. The latter are determined as follows. The d components Π_d^\pm are given by

$$\Pi_d^\pm = \frac{1}{2} (P_2^d \pm P_1^d),$$

$$\begin{aligned} P_1^d(\mathbf{q}, i\omega_n) &= \frac{t_0^2}{2} \sum_{+,-} \sum_{\mathbf{k}} (M_{\mathbf{k}-\mathbf{q}, \mathbf{q}}^d)^2 \frac{n^F(E_{\mathbf{k}-\mathbf{q}}^\pm) - n^F(E_{\mathbf{k}}^\pm)}{i\omega_n + E_{\mathbf{k}-\mathbf{q}}^\pm - E_{\mathbf{k}}^\pm}, \\ P_2^d(\mathbf{q}, i\omega_n) &= \frac{t_0^2}{2} \sum_{+,-} \sum_{\mathbf{k}} (M_{\mathbf{k}-\mathbf{q}, \mathbf{q}}^d)^2 \frac{n^F(E_{\mathbf{k}-\mathbf{q}}^\pm) - n^F(E_{\mathbf{k}}^\mp)}{i\omega_n + E_{\mathbf{k}-\mathbf{q}}^\pm - E_{\mathbf{k}}^\mp}, \end{aligned} \quad (55)$$

where P_1 and P_2 are due to decay of the d -magnon into two fermions belonging to the same and different branches, respectively. These expressions correspond to the bubble graph for $\Pi_d^+ \equiv \Pi_{dd^+}$, defined analytically as

$$\begin{aligned} \Pi_d^+(\mathbf{q}, i\omega_n) &= t_0^2 \sum_{\mathbf{k}} \sum_{\omega_n} [(M_{\mathbf{k}-\mathbf{q}, \mathbf{q}}^d)^2 \\ &\quad \times K_{11}(\mathbf{k} - \mathbf{q}, i\omega_{m-n}) K_{22}(\mathbf{k}, i\omega_m)], \end{aligned} \quad (56)$$

and to the similar bubble graph and similar analytical expression for $\Pi_d^- \equiv -\Pi_{dd^-}$; they are obtained after summation over imaginary frequency $i\omega_n$. The expressions for the c components Π_c^\pm have the same structure as (55) with M^d replaced by M^c . For the “mixed” components Π_{cd}^\pm one should replace in (55) $(M^d)^2$ by $M^d M^c$ [85].

The above written expressions describe the renormalization of the magnon Green functions. To get expressions for the renormalized spin Green functions, we have to use the expressions for the S^α operators through the a, b operators, of the latter through the c, d operators and the symmetry properties of the magnon Green functions. After a bit long but straightforward calculations, we get the following expressions relating the renormalized spin Green functions \tilde{G}_s^{xx} and \tilde{G}_s^{yy} to the renormalized magnon Green functions:

$$\begin{aligned} \tilde{G}_s^{yy}(\mathbf{q}, i\omega_n) &= \frac{1}{2} F_{\mathbf{q}}^c \{ [\tilde{G}_{cc^+}(\mathbf{q}, i\omega_n) + \tilde{G}_{c+c}(\mathbf{q}, i\omega_n)] \\ &\quad - [\tilde{G}_{cc}(\mathbf{q}, i\omega_n) + \tilde{G}_{c+c^+}(\mathbf{q}, i\omega_n)] \}, \end{aligned} \quad (57)$$

$$\tilde{G}_s^{xx}(\mathbf{q}, i\omega_n) = \frac{1}{2} [R(\mathbf{q} + \mathbf{Q}, i\omega_n) + R(\mathbf{q} - \mathbf{Q}, i\omega_n)], \quad (58)$$

where

$$R(\mathbf{q}, i\omega_n) = \frac{1}{2} F_q^d \{ [\tilde{G}_{dd^+}(\mathbf{q}, i\omega_n) + \tilde{G}_{d+d}(\mathbf{q}, i\omega_n)] + [\tilde{G}_{dd}(\mathbf{q}, i\omega_n) + \tilde{G}_{d+d^+}(\mathbf{q}, i\omega_n)] \} \quad (59)$$

(the multimagnon contribution is neglected). Note that the terms related to the c (d) operators cancel each other in the expression for \tilde{G}_s^{xx} (\tilde{G}_s^{yy}) and the terms containing one c and one d operators cancel each other in the expressions for both \tilde{G}_s^{xx} and \tilde{G}_s^{yy} . As a consequence, even being renormalized due to the spin-charge interaction, the out-of-plane spin Green function \tilde{G}_s^{yy} remains sensitive only to the optical mode, while

$$\begin{aligned} (\tilde{G}_{cc^+} + \tilde{G}_{c^+c})(\mathbf{q}, i\omega_n) &= (\tilde{G}_{dd^+} + \tilde{G}_{d+d})(\mathbf{q}, i\omega_n) \\ &= 2 \frac{[\omega_q(\omega_q + 2\Pi_q^+(i\omega_n)) - (i\omega_n)^2](\omega_q + 2\Pi_q^+(i\omega_n)) - (2\Pi_q^-(i\omega_n))^2 \omega_q}{D(\mathbf{q}, i\omega_n)}, \end{aligned} \quad (60)$$

$$(\tilde{G}_{cc} + \tilde{G}_{c^+c^+})(\mathbf{q}, i\omega_n) = (\tilde{G}_{dd} + \tilde{G}_{d+d^+})(\mathbf{q}, i\omega_n) = -\frac{4(i\omega_n)^2 \Pi_q^-(i\omega_n)}{D(\mathbf{q}, i\omega_n)}, \quad (61)$$

with the determinant given by

$$D(\mathbf{q}, i\omega_n) = [(i\omega_n)^2 - \omega_q(\omega_q + 2P_1(\mathbf{q}, i\omega_n))] \times [(i\omega_n)^2 - \omega_q(\omega_q + 2P_2(\mathbf{q}, i\omega_n))]. \quad (62)$$

The renormalized spectra of the two magnon modes are given by solutions of the equation $D(\mathbf{q}, \omega) = 0$ on the real axis. They are explicitly described by the equations

$$\begin{aligned} \tilde{\Omega}_q^d &= \sqrt{\omega_q[\omega_q + 2P_2(\mathbf{q}, \tilde{\Omega}_q^d)]}, \\ \tilde{\Omega}_q^c &= \sqrt{\omega_q[\omega_q + 2P_1(\mathbf{q}, \tilde{\Omega}_q^c)]}. \end{aligned} \quad (63)$$

Note that (63) are not expressions but equations with respect to $\tilde{\Omega}_q^{c,d}(\omega)$ that should be solved self-consistently [in Eq. (63) the argument ω is omitted].

Using (60)–(62), we obtain the following: for the out-of-plane spin Green function the expression

$$\tilde{G}_s^{yy}(\mathbf{q}, i\omega_n) = F_q \frac{\omega_q + 2P_1(\mathbf{q}, i\omega_n)}{\omega^2 - \omega_q[\omega_q + 2P_1(\mathbf{q}, i\omega_n)]}, \quad (64)$$

and for the in-plane spin Green function the expression of the form (58) with $R(\mathbf{q}, i\omega_n)$ given by

$$R(\mathbf{q}, i\omega_n) = F_q \frac{\omega_q + 2P_2(\mathbf{q}, i\omega_n)}{\omega^2 - \omega_q[\omega_q + 2P_2(\mathbf{q}, i\omega_n)]}, \quad (65)$$

where $F_q = F_q^c = F_q^d$ [defined after Eqs. (25) and (26)]. Note that despite the degeneracy between the bare Goldstone and optical modes in this limit, the two modes finally remain distinguishable due to the presence of the different polarization-operator components in the renormalized spectra.

(2) Another limit in which the inversion of the matrix (54) is simplified is $q' \ll \sqrt{2}\bar{\Delta}^c$. In this case, one can neglect the mixed components of the polarization operator with respect to the pure components and consider the two modes separately,

the in-plane Green function \tilde{G}_s^{xx} does only to the Goldstone mode.

To calculate explicitly the Green functions we have first to invert the 4×4 matrix (54) with frequency dependent components. This is a quite difficult problem. The procedure is simplified in the following cases.

(1) In the limit $q' \gg \sqrt{(2)}\bar{\Delta}^c$. In this case, the bare magnon spectra and the scattering amplitudes for the d and c modes tend to each other, $\Omega_q^d \sim \Omega_q^c \sim \omega_q$, $M^d \sim M^c$. Then, the polarization operator components become approximately equal as well: $P_{1,2}^c \sim P_{1,2}^d \sim P_{1,2}^d \equiv P_{1,2}$ and the expressions for the magnon Green functions, magnon spectra, and spin Green functions are simplified. Namely we get for the magnon Green functions:

i.e., represent the polarization operator as

$$\hat{\Pi} = \begin{bmatrix} \hat{\Pi}^d & \hat{0} \\ \hat{0} & \hat{\Pi}^c \end{bmatrix}, \quad (66)$$

$$\hat{\Pi}^d = \begin{bmatrix} \Pi_{dd^+} & \Pi_{dd} \\ \Pi_{d+d^+} & \Pi_{d+d} \end{bmatrix}, \quad \hat{\Pi}^c = \begin{bmatrix} \Pi_{cc^+} & \Pi_{cc} \\ \Pi_{c^+c^+} & \Pi_{c^+c} \end{bmatrix}. \quad (67)$$

For the Goldstone mode, this approximation is valid under the additional condition $(k_F^-)^4 \ll \sqrt{q'}/\bar{\Delta}^c$, see comment in [86].

Performing explicit calculations we get for the magnon Green functions corresponding to the block $\hat{\Pi}^d$ the following expressions:

$$\begin{aligned} \tilde{G}_{dd^+}(\mathbf{q}, i\omega_n) &= \tilde{G}_{d+d}(\mathbf{q}, -i\omega_n) \\ &= \frac{\Omega_q^d + \Pi_d^+(\mathbf{q}, i\omega_n) + i\omega_n}{D^d(\mathbf{q}, i\omega_n)}, \end{aligned} \quad (68)$$

$$\tilde{G}_{dd}(\mathbf{q}, i\omega_n) = \tilde{G}_{d+d^+}(\mathbf{q}, i\omega_n) = \frac{\Pi_d^-(\mathbf{q}, i\omega_n)}{D^d(\mathbf{q}, i\omega_n)}, \quad (69)$$

$$D^d(\mathbf{q}, i\omega_n) = (i\omega_n)^2 - [\Omega_q^d + P_1^d(\mathbf{q}, i\omega_n)] \times [\Omega_q^d + P_2^d(\mathbf{q}, i\omega_n)], \quad (70)$$

and similar expressions for the Green functions corresponding to the block $\hat{\Pi}^c$ obtained when replacing the index d by c everywhere in (68)–(70). The solutions of the equations $D^d(\mathbf{q}, \omega) = 0$, $D^c(\mathbf{q}, \omega) = 0$ on the real axis (if they exist) determine the renormalized spectrum of the d and c modes in this limit:

$$\begin{aligned} \tilde{\Omega}_q^d &= \sqrt{[\Omega_q^d + P_1^d(\mathbf{q}, \tilde{\Omega}_q^d)][\Omega_q^d + P_2^d(\mathbf{q}, \tilde{\Omega}_q^d)]}, \\ \tilde{\Omega}_q^c &= \sqrt{[\Omega_q^c + P_1^c(\mathbf{q}, \tilde{\Omega}_q^c)][\Omega_q^c + P_2^c(\mathbf{q}, \tilde{\Omega}_q^c)]}, \end{aligned} \quad (71)$$

those are not expressions but equations [with respect to $\tilde{\Omega}_q^{c,d}(\omega)$] that should be solved self-consistently.

Using (68)–(70), we get for the out-of-plane spin Green function in this limit,

$$\tilde{G}_s^{yy}(\mathbf{q}, i\omega_n) = F_{\mathbf{q}}^c \frac{\Omega_{\mathbf{q}}^c + P_1^c(\mathbf{q}, i\omega_n)}{(i\omega_n)^2 - [\Omega_{\mathbf{q}}^c + P_1^c(\mathbf{q}, i\omega_n)][\Omega_{\mathbf{q}}^c + P_2^c(\mathbf{q}, i\omega_n)]}, \quad (72)$$

while for the in-plane spin Green function \tilde{G}_s^{xx} we get again the general structure (58) in which $R(\mathbf{q}, i\omega_n)$ is written as

$$R(\mathbf{q}, i\omega_n) = F_{\mathbf{q}}^d \frac{\Omega_{\mathbf{q}}^d + P_2^d(\mathbf{q}, i\omega_n)}{(i\omega_n)^2 - [\Omega_{\mathbf{q}}^d + P_1^d(\mathbf{q}, i\omega_n)][\Omega_{\mathbf{q}}^d + P_2^d(\mathbf{q}, i\omega_n)]}. \quad (73)$$

The corresponding static susceptibilities are given by

$$\begin{aligned} \chi^{xx}(\mathbf{q}, 0) &\propto \frac{F_{\mathbf{q}+\mathbf{Q}}^d}{[\Omega_{\mathbf{q}+\mathbf{Q}}^d + P_1^d(\mathbf{q} + \mathbf{Q}, 0)]} + (Q \rightarrow -Q), \\ \chi^{yy}(\mathbf{q}, 0) &\propto \frac{F_{\mathbf{q}}^c}{\Omega_{\mathbf{q}}^c + P_2^c(\mathbf{q}, 0)}, \end{aligned} \quad (74)$$

so that the in-plane static susceptibility diverges as $\chi^{xx} \propto [\frac{1}{(q'+\mathbf{Q})^2} + \frac{1}{(q'-\mathbf{Q})^2}]$ like in the spin wave approximation described in Sec. IV. Here, we took into account that $F_{\mathbf{q} \pm \mathbf{Q}}^d \propto \frac{1}{\Omega_{\mathbf{q} \pm \mathbf{Q}}^d}$.

3. In the limit $q' \sim \sqrt{2}\bar{\Delta}^c$ calculations are also simplified. The \mathbf{q} dependencies of the M^c and M^d amplitudes become the same—both are proportional to q' while $\frac{(M^c)^2}{(M^d)^2} \sim \frac{1}{\sqrt{1+\zeta}}$. As a result, the polarization operators Π_d^+ , Π_c^+ , Π_{cd}^+ , as well as Π_d^- , Π_c^- , Π_{cd}^- , have the same functional dependencies and differ only by the numerical factors related to the amplitudes. In this case one can reduce the 4×4 matrix \hat{G} to the effective 2×2 matrix \hat{G}^{eff} in the way shown in Appendix. As follows from the present there formulas, the equations for the renormalized magnon spectrum can explicitly be written as

$$\omega^2 = \frac{\omega_1^2 + \omega_2^2}{2} \pm \sqrt{\left(\frac{\omega_1^2 - \omega_2^2}{2}\right)^2 + A}, \quad (75)$$

where

$$\begin{aligned} \omega_1^2 &= (\tilde{\Omega}^d + P_1^d)(\tilde{\Omega}^d + P_2^d) - P_2^c P_1^d, \\ \omega_2^2 &= (\tilde{\Omega}^c + P_1^c)(\tilde{\Omega}^c + P_2^c) - P_1^c P_2^d, \\ A &= [(\tilde{\Omega}^d + P_2^d)P_1^c - (\tilde{\Omega}^c + P_1^c)P_2^c] \\ &\quad \times [(\tilde{\Omega}^c + P_2^c)P_1^d - (\tilde{\Omega}^d + P_1^d)P_2^d] \end{aligned}$$

(we omit the argument \mathbf{q}, ω in $\tilde{\Omega}^d, \tilde{\Omega}^c$ and $P_{1,2}^{c,d}$ for short). Again, the formulas (75) are not expressions but equations that should be solved self-consistently. Note that in this limit, it is enough to calculate explicitly P_1^d components, the P_1^c components will differ only by factor $\frac{1}{\sqrt{1+\zeta}}$ in the right-hand side (rhs).

The expressions for the spin Green functions are very cumbersome in this limit, we do not present them. We note only that they have the structure general for all the limits:

$$\tilde{G}_s^{xx}(\mathbf{q}, \omega)_s = \frac{1}{2}[R(\mathbf{q} + \mathbf{Q}, \omega) + R(\mathbf{q} - \mathbf{Q}, \omega)],$$

$$R(\mathbf{q}, \omega) = \frac{N^d(\mathbf{q}, \omega)}{D_\omega(\mathbf{q})}, \quad \tilde{G}_s^{yy}(\mathbf{q}, \omega)_s = \frac{N^c(\mathbf{q}, \omega)}{D_\omega(\mathbf{q})} \quad (76)$$

with D_ω given in Appendix, whose behavior determines the main features of the spin dynamics.

B. Properties of the polarization operator and an impact of its structure on the renormalized spin fluctuation spectra

In this section, we calculate the polarization operator components. Near the AF boundary, calculations can be performed analytically since the main contribution to the integrals (55) comes from the momenta in the vicinities of the minima in the hole spectra and therefore one can use quadratic expansions for $E_{\mathbf{k}}^\pm$, while for the scattering amplitude one can write explicitly

$$\begin{aligned} (M_{\mathbf{k}-\mathbf{q}, \mathbf{q}}^d)^2 &\approx \frac{\sqrt{1+\zeta}}{8} \frac{(q'_x \sin(k_x + Q_x) + q'_z \sin(k_z + Q_z))^2}{q'}. \end{aligned} \quad (77)$$

Below, we will omit everywhere the ‘‘prime’’ in \mathbf{q}' , $\mathbf{q}' \rightarrow \mathbf{q}$, i.e., consider \mathbf{q} defined with respect to the AF wave vector \mathbf{Q}_{AF} , and $q = |\mathbf{q}|$.

To perform explicit calculations, we have to fix the symmetry of the spiral state. We will consider the spiral state of the uniaxial (1,0) symmetry, $Q_x = Q$, $Q_z = 0$, since first, it is energetically favorable with respect to the (1,1) state, as was shown in earlier papers [42,47–49] and confirmed by our calculations (Sec. VI) and second, it is this symmetry that is observed experimentally in the magnetically ordered incommensurate state in low-doped cuprates. Analytical calculations give for this case the following expressions for P_1^d and P_2^d (for one chosen pocket):

$$\begin{aligned} \text{Re} P_2^d(\mathbf{q}, \omega) &= \Lambda \frac{q_1 \sqrt{\alpha}}{q} \{ [-\omega_+^\Delta + \text{sgn}(\omega_+^\Delta) F((\omega_+^\Delta)^2 - (2k_F^-)^2)] \\ &\quad + [\omega_-^\Delta - \text{sgn}(\omega_-^\Delta) F((\omega_-^\Delta)^2 - (2k_F^-)^2)] \\ &\quad + [-\omega_+^{-\Delta} + \text{sgn}(\omega_+^{-\Delta}) F((\omega_+^{-\Delta})^2 - (2k_F^+)^2)] \\ &\quad + [\omega_-^\Delta - \text{sgn}(\omega_-^\Delta) F((\omega_-^\Delta)^2 - (2k_F^+)^2)] \}, \\ \text{Im} P_2^d(\mathbf{q}, \omega) &= \Lambda \frac{q_1 \sqrt{\alpha}}{q} \{ [F((2k_F^-)^2 - (\omega_+^\Delta)^2) - F((2k_F^-)^2 - (\omega_-^\Delta)^2)] \\ &\quad + [F((2k_F^+)^2 - (\omega_+^{-\Delta})^2) - F((2k_F^+)^2 - (\omega_-^\Delta)^2)] \}, \end{aligned} \quad (78)$$

where

$$\begin{aligned} F(X) &= \theta(X) \sqrt{X}, \quad \omega = \omega_\pm + \Delta/a\bar{q}, \quad \omega_\pm^{-\Delta} = \omega_\pm - \Delta/a\bar{q}, \\ \omega_\pm &= \omega/a\bar{q} \pm \bar{q}, \quad \bar{q} = q_1/\sqrt{\alpha}, \\ \alpha &= \left(1 + \frac{b q_2^2}{a q_1^2}\right)^{-1}, \quad \Lambda = \frac{t^2}{2\pi \sqrt{(1+\zeta)ab}}. \end{aligned} \quad (79)$$

The expressions for P_1^d are given by (78), (79) when setting $\Delta = 0$,

$$P_1^d(\mathbf{q}, \omega) = P_2^d(\mathbf{q}, \omega, \Delta = 0). \quad (80)$$

In (78) and (79), Δ is the fermion gap at the minima of the fermion spectrum, $\Delta = 2|B_{\mathbf{k}=(\pi/2,\pi/2)}| = 2tQ$, q_1, q_2 are respectively the \mathbf{q} components orthogonal and parallel to the AF BZ boundary near the considered pocket, $\theta(X)$ is the Heaviside theta function, Λ is the effective interaction, $k_F^\pm = \sqrt{\pi n^\pm} \epsilon$ are the Fermi wave vectors in the direction perpendicular to the AF boundary for $E_{\mathbf{k}}^\pm$ branches, respectively, where $n^\pm = (1/N) \sum_{\mathbf{k}} n^F(E_{\mathbf{k}}^\pm - \mu)$ are the populations of these branches and $\epsilon = \sqrt{b/a}$. (When calculating we used for the scattering amplitude $|M_{\mathbf{k}-\mathbf{q},\mathbf{q}}^d|^2 \approx |M^d|^2$ where $|M^d|^2$ is the amplitude at the fermion spectra minimum $\mathbf{k} = (\pi/2, \pi/2)$; we neglect the small changes in the fermion effective masses due to the term $B_{\mathbf{k}}$ and the weak momentum dependence of the electron gap, fixing its value at the minimum of hole dispersion.) Note that the case of a formally negative $(k_F^+)^2$ (when calculated as $(k_F^+)^2 = (k_F^-)^2 - \Delta/a$) corresponds to the unpopulated $E_{\mathbf{k}}^+$ branch, and k_F^+ should be set equal to zero in (78) in this case. The expressions (78) and (79) are written for one pocket. The global expressions for $P_{1,2}^d$ contain a sum over four pockets. Note that for the pockets centered at $(\pi/2, \pi/2)$, $(-\pi/2, -\pi/2)$, the q_1 component of \mathbf{q} is parallel to the (1, 1) direction while for the pockets centered at $(-\pi/2, \pi/2)$, $(\pi/2, -\pi/2)$, the q_1 component is parallel to the (1, -1) direction.

Note that in the limit $Q = 0$, the expressions for P_2^d and P_1^d coincide, $P_2^d = P_1^d$. Since k_F^+ and k_F^- in Eq. (78) coincide as well, the expressions (78) and (79) are reduced to those obtained earlier for the doped AF state, see Ref. [69]. Note also that in the latter case the interaction Λ is higher than in the spiral state when calculated with the same parameter values, namely it is twice higher than in the spiral state with only the lowest branch $E_{\mathbf{k}}^-$ filled. In other words, in such a spiral state, the effect of the electron-spin interaction is twice reduced with respect to the collinear AF state. As a consequence, the Goldstone mode, whose instability is at the origin of the instability of the AF state above a certain, quite low, critical hole concentration n_c^{AF} [69,87,88], remains stable for $n > n_c^{\text{AF}}$ when the order is spiral.

The expressions (78) and (79) are written for the d components of the polarization operator. We remind the reader that in the limit $q' \gg \sqrt{2}\bar{\Delta}^c$, the d and c components of the polarization operators coincide, $P_{1,2}^c = P_{1,2}^d$, and that in the limit $q' \sim \sqrt{2}\bar{\Delta}^c$ they differ only by a numerical factor while having the same ω, \mathbf{q} dependencies: $P_{1,2}^c = \frac{1}{\sqrt{1+\zeta}} P_{1,2}^d$. Below, we will omit the superscript d in the polarization operators $P_{1,2}^d$ for short.

The knowledge of the analytical form of the momentum and energy dependencies of the polarization operator allows us to get formulas for certain characteristic lines whose location in the ω - \mathbf{q} plane largely determines the form of spin fluctuation dispersion, as we will see later on. These lines are given by the equations

$$\begin{aligned} \omega_1(\mathbf{q}) &= a\bar{q}(2k_F^- - \bar{q}), & \omega_2(\mathbf{q}) &= a\bar{q}(\bar{q} - 2k_F^-), \\ \omega_3(\mathbf{q}) &= a\bar{q}(2k_F^- + \bar{q}), \end{aligned} \quad (81)$$

for P_1 and

$$\omega_2^\Delta(\mathbf{q}) = a\bar{q}(\bar{q} - 2k_F^-) + \Delta, \quad \omega_3^\Delta(\mathbf{q}) = a\bar{q}(2k_F^- + \bar{q}) + \Delta \quad (82)$$

for P_2 , see Ref. [89]. First, they are the lines of square-root singularities in the real and imaginary parts of P_1 and P_2 . Second, they are the lines of onset of $\text{Im}P_l \neq 0$, namely, $\text{Im}P_1$ is nonzero only in the area between the lines $\omega_2(\mathbf{q})$ and $\omega_3(\mathbf{q})$, while $\text{Im}P_2$ is nonzero in the area between $\omega_2^\Delta(\mathbf{q})$ and $\omega_3^\Delta(\mathbf{q})$. We will call the latter areas Cont1 and Cont2, respectively (that stands for the continuum 1 and continuum 2), to emphasize that in these areas there is a two-particle electron-hole contribution to the spin susceptibility in addition to the one-particle contribution from localized spins. Depending on parameters, the locations of these lines and of the Cont1 and Cont2 can vary significantly, see Fig. 2. Figure 2(a) corresponds to the case when only the lower fermion branch $E_{\mathbf{k}}^-$ is filled—in this case, the Cont2 lies entirely at positive ω . Figures 2(b) and 2(c) correspond to the case when the $E_{\mathbf{k}}^+$ band is also filled—the Cont2 descends into negative ω ; in Fig. 2(b), the fillings of the two branches differ significantly, in Fig. 2(c), the filling of the branch E^+ approaches the filling for E^- . The limit $n^+ = n^-$, $k_F^+ = k_F^-$ corresponds to the AF state: the blue and black lines in Fig. 2 coincide. For parameters typical for cuprates (which we discuss in the following subsection), the situation is at the limit between the cases in Figs. 2(a) and 2(b). A reader can already take a look of Fig. 3 plotted for parameters typical for cuprates in which the Cont2 related to the polarization operator P_2 is shown by orange color and the Cont1 related to P_1 by grey.

Outside the two continua, the bosonic excitations have no damping. The renormalization of their spectrum with respect to the noninteracting spin-wave spectrum and of their spectral weight are determined by $\text{Re}P_1$ and $\text{Re}P_2$. Since the latter have square-root singularities at the borders of the continua, the quasiparticle spectral weight diminishes in approaching any continua border and vanishes on it. Schematically, it is seen from the following: outside the continua, the susceptibility can be written as $\text{Im}\chi_{\text{res}}(\mathbf{q}, \omega) = a_{\mathbf{q}}\delta(\omega - \tilde{\Omega}_{\mathbf{q}})$ with a spectral weight given by $a_{\mathbf{q}} = \frac{\tilde{\Omega}_{\mathbf{q}}}{\tilde{\Omega}_{\mathbf{q}}} \{1 - \frac{\tilde{\Omega}_{\mathbf{q}}}{\tilde{\Omega}_{\mathbf{q}}} [\frac{\partial P(\mathbf{q}, \omega)}{\partial \omega} |_{\omega=\tilde{\Omega}_{\mathbf{q}}}] \}^{-1}$ ($\tilde{\Omega}_{\mathbf{q}}$ and $\tilde{\tilde{\Omega}}_{\mathbf{q}}$ are bare and renormalized dispersions respectively and P is a polarization operator at the origin of the renormalization), so that $a_{\mathbf{q}}$ is zero at the point where P exhibits a square-root singularity. As to the renormalization of the dispersion, the properties of P_1 , and P_2 are such that the low-energy part of the Goldstone mode should obligatory soften with respect to the spin-wave spectrum. Indeed, as follows from Eq. (78), the $\text{Re}P_l$ is negative below (in ω) the continuum Cont l and therefore if acted alone, $\text{Re}P_l$ ($l = 1$ or $l = 2$) would tend to soften the dispersion when the spin-wave spectrum lies below the Cont l . Since the bare Goldstone mode $\tilde{\Omega}_{\mathbf{q}}$ in its initial part (low ω , low q) lies obligatory below Cont2 and on the other hand for such q, ω , $|\text{Re}P_2|$ is much higher than $|\text{Re}P_1|$, the renormalized dispersion of the Goldstone mode $\tilde{\tilde{\Omega}}^d$ should soften with respect to the spin-wave dispersion $\tilde{\Omega}^d$.

Inside the continua the form of SF spectra is settled by a competition between one-particle (magnon) and two-particle (electron-hole) contributions. We will see later on that inside the Cont2, the two-particle processes can even dominate the spin dynamics (that happens for parameters typical for cuprates) so that it becomes of the relaxation type. Since due to the square-root singularities, $\text{Im}P_l$ and $\text{Re}P_l$ behave in a quite sharp way near the borders, some sort of pinning of

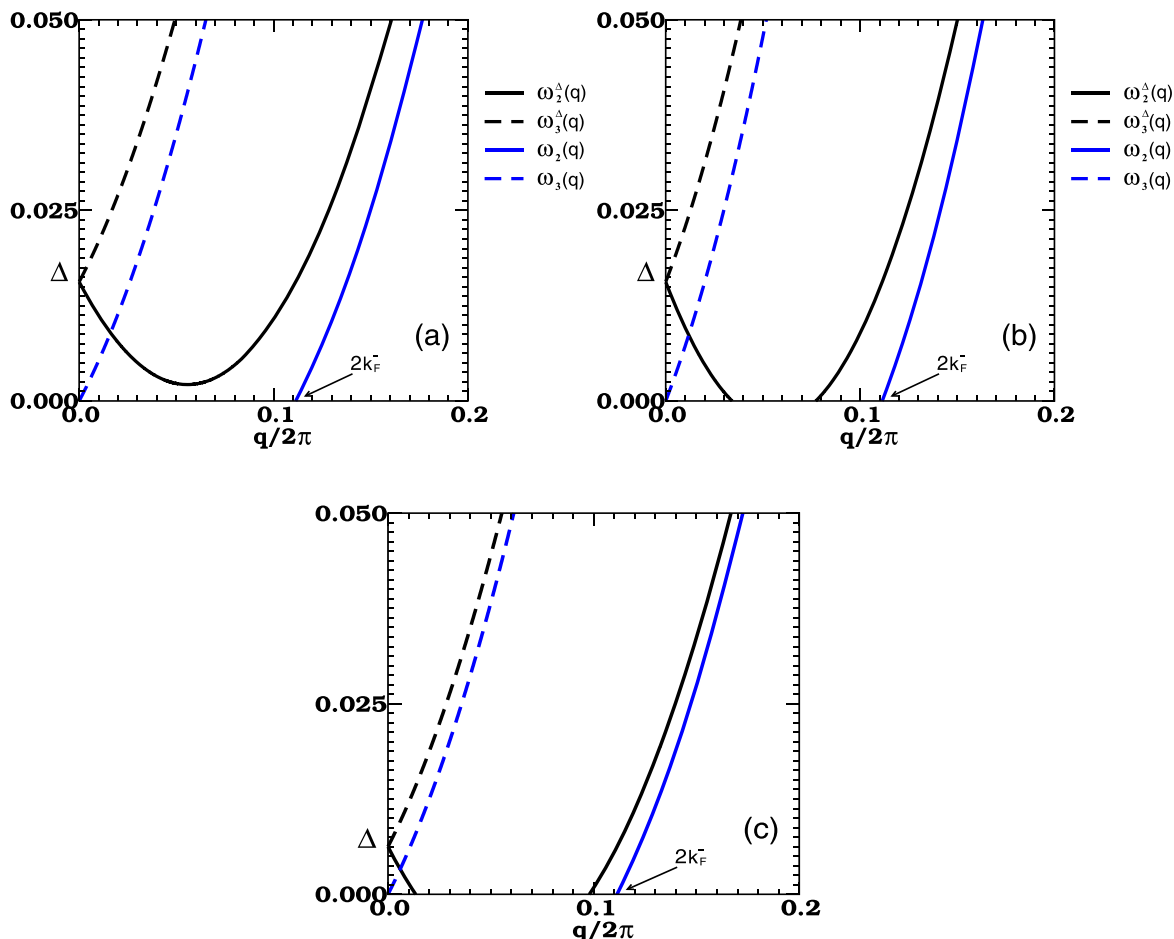


FIG. 2. Possible locations in the energy-momentum space of the characteristic lines $\omega_2(q)$, $\omega_3(q)$, $\omega_2^\Delta(q)$, and $\omega_3^\Delta(q)$ [Eqs. (81) and (82)] and of the two continua, Cont1 and Cont2 [corresponding to the areas between the $\omega_2(q)$, $\omega_3(q)$ lines and the $\omega_2^\Delta(q)$, $\omega_3^\Delta(q)$ lines, respectively]. In fact, (a) and (b) are plotted for the parameter values characteristic for cuprates and Q obtained self-consistently for $n = 0.04$, they differ only by the values of the inverse effective hole mass a in Eq. (31): (a) $a = 0.11$ eV and (b) 0.15 eV that are, respectively, slightly lower and higher than the estimated limits for a (see Sec. VI A). The plot (c) shows the tendency of evolution with decreasing Q , i.e., with approaching the collinear AF state; in the limit $Q \rightarrow 0$, there is a degeneration, and the blue and black lines coincide. The plots correspond to the (1,0) direction [for the (1,0) spiral state]; the wave vectors are defined with respect to \mathbf{Q}_{AF} and q stands for q_x , $q \equiv q_x$. The energies are in eV.

incoherent SFs spectra to one of the continua's border will occur in this case.

VI. SPIN FLUCTUATIONS IN CUPRATES

A. Spiral-state spin fluctuations for parameter values typical for cuprates

Let us now apply the developed above general formulation to cuprates. For this, we have to fix the parameter values and then to perform self-consistent calculations based on the obtained equations. First, the incommensurability wave vector \mathbf{Q} should be determined self-consistently. This can be done by minimizing the free energy, i.e., from the equation $\frac{\partial E}{\partial \mathbf{Q}} = 0$ (for $T = 0$). The spin contribution E_s to E equals to $E_s = -NJ_Q/8$ (for simplicity, we keep only the dominant term neglecting “zero-point” fluctuations having usually a very small density). The hole contribution E_h is given by $E_h = \sum_{\mathbf{k}, \pm} E_{\mathbf{k}}^\pm n^F(E_{\mathbf{k}}^\pm - \mu)$. When taking into account the explicit expressions for $E_{\mathbf{k}}^\pm$ [Eq. (38)], we get for the (1,0) spiral state

($\mathbf{Q} = (Q, 0)$): $E_h^{(1,0)} = -QtN(n_- - n_+) + \sum_{\mathbf{k}} \epsilon_{\mathbf{k}}(n_{\mathbf{k}}^- + n_{\mathbf{k}}^+)$ so that for the total energy, we have

$$E^{(1,0)}/N = -J_Q/8 - Qt(n_- - n_+) + \pi(n_+^2 + n_-^2)\sqrt{ab}, \quad (83)$$

$n_\pm = (1/N) \sum_{\mathbf{k}} n^F(E_{\mathbf{k}}^\pm - \mu)$ are the populations of the $E_{\mathbf{k}}^\pm$ bands; the total hole concentration is $n = n_- + n_+$. [This energy is lower than the energy of the (1,1) spiral state $E^{(1,1)}/N$, as seen from similar calculations for the latter state and as known from earlier papers.] When $n^+ \ll n^-$ (that is always the case for the parameter values discussed below), we get for the spiral incommensurability wave vector in the (1,0) state, $Q = \frac{4t}{J}(n^- - n^+) \approx \frac{4t}{J}n$.

Second, one should take into account a renormalization of the charge parameters. Such a renormalization appears due to the spin-hole interaction $H_{s-h}^{(3)}$. The latter leads to the fermion self-energy, which in shorthand notations is written as $\hat{\Sigma} = M^2 \hat{K} \hat{G}$ so that the renormalized matrix fermion Green function is given by $(\hat{K})^{-1} = \hat{K}^{-1} - \hat{\Sigma}$. We will not perform

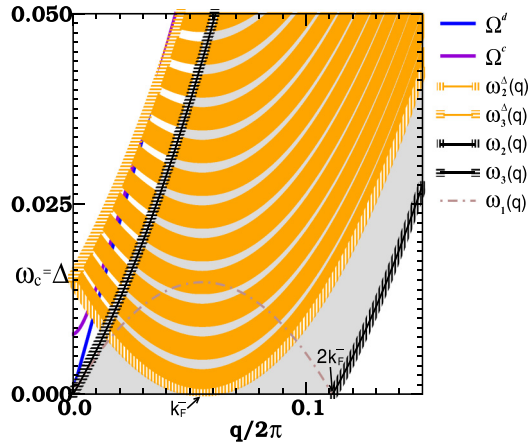


FIG. 3. The two branches of the bare boson spectrum, $\Omega^d(q)$ and $\Omega^c(q)$, and the two continua, Cont1 and Cont2, for the parameters typical for cuprates and $n = 0.04$ (plotted in the ω - \mathbf{q} space near AF wave vector, the energies are in eV). (The parameter values are given in Sec. VI A.) The grey and orange shaded areas show the continua Cont1 and Cont2 associated with the two-particle “electron-hole” fluctuations originated from the fermions of the same and different branches respectively. Other notations are as in Fig. 2.

explicit calculations to get the renormalized charge parameters. We expect that the renormalization should be similar to that in the commensurate AF state. It was shown [74–80] that the dressing of holes on the AF background reduces the bandwidth by a factor Z_h , which is of the order of J/t , while the hole dispersion is as in Eq. (30). The parameters of the dressed-hole dispersion for the t - J model with only nn hopping were obtained in Refs. [74–78], later on they were recalculated taking into account the bare hopping beyond nn [79,80]. The absolute values of x_1, x_2 [Eq. (30)], or equivalently of a, b [Eq. (31)], depend on J/t ; for reasonable for cuprates values, $J = 0.125$ eV, $t/J = 2.5$, and an estimated range for $t', t'', t' = -(0.25 - 0.35)t, t'' = (0.12 - 0.16)t$, the latter estimations give $a \sim 0.12 - 0.14$ eV and $\epsilon = \sqrt{b/a} \sim 1$. (These estimations correspond very well to the experimental data for the dispersion of a hole on the AF background [90,91].) The part of the hole spectrum with $B_{\mathbf{k}}$ also should be renormalized: $B_{\mathbf{k}} \rightarrow Z_h^B B_{\mathbf{k}}$. Then, the first term in the expression for $E_h^{(1,0)}$ is renormalized by the factor Z_h^B as well, and the equation for Q becomes $Q = (4tZ_h^B/J)n$. The fermionic gap is renormalized as well: $\Delta = 2Z_h^B t Q$. We suppose that Z_h^B is also of the order of J/t . Further, since in fact it is not J but the Goldstone mode velocity that participates in the renormalization of the hole spectrum, and since this velocity is lowering significantly in the renormalized spin spectrum, we should use for the estimations of Z_h^B the effective J corresponding to the renormalized velocity. (The effect of the softening of the Goldstone mode is explained qualitatively in Sec. V B and obtained numerically in this section, see below.) Incorporating this effect we take $Z_h^B \sim 0.25$ and correspondingly $Q \sim 2.5n$. And finally, one should take into account a renormalization of the fermion quasiparticle residue—by a factor Z_{res} . This leads to the appearance of the factor Z_{res}^2 in the expression for the polarization operator that can be incorporated in the effective interaction Λ : $\Lambda \rightarrow$

ΛZ_{res}^2 . The estimated range for Z_{res} is $0.35 - 0.4$. We will use $Z_{\text{res}} = 0.38$ as in [76]. The last parameter we need for numerical calculations is the exchange-interaction anisotropy: we use $1 - \zeta = 0.003$, that is, of the same order that observed experimentally [53–56].

The results of calculations performed with these parameters for the hole concentration $n = 0.04$ are presented in Figs. 3–6. First, in Fig. 3, we show the two branches of the bare boson spectra [Eqs. (18) and (19)] and the two continua, Cont1 and Cont2. The locations of the continua in this and the following figures correspond to $a = 0.12$ eV, which is the low limit of the estimated range $a = 0.12 - 0.14$ eV. For higher values of a , Cont2 moves down into negative ω area (the tendencies see in Fig. 2), and the discussed below effects are even more pronounced. The plot in Fig. 3 (and in the following figures) corresponds to the (1,0) direction [for the spiral of the (1,0) symmetry]; in this case $\bar{q} = q_x/\sqrt{2\alpha}, k_F^\pm = (k_F^\pm)_x/\sqrt{2\alpha}$, where q_x and $(k_F^\pm)_x$ are the components of \mathbf{q} and \mathbf{k}_F^\pm in the (1,0) direction. Since we took the spectrum of the dressed holes practically isotropic, we have $\alpha = 1/2$ and therefore $\bar{q} = q_x$ in the equations (78) and (79). Below we denote $q_x \equiv q$. Self-consistent calculations of the renormalized spectra show that the most important consequences of the dynamic spin-charge interaction concern the in-plane fluctuations while the dispersion of the mode Ω^c is roughly conserved, see Ref. [92]. The renormalized boson spectrum associated with the in-plane fluctuations is presented in Fig. 4. The first remarkable feature is that the low-energy fluctuations keep a resonant character only in a small area in the q - ω space, see the magenta line with square symbols. Of course, in the limit $\omega \rightarrow 0, q \rightarrow 0$, the resonance mode still has a linear dispersion, $\tilde{\Omega}^d = \tilde{c}q$, as it should be in a correspondence to the Goldstone theorem while the velocity is strongly reduced, $\tilde{c} < c$, (see the discussion in the end of Sec. V B). The Goldstone mode lies slightly above the Cont1. It is accompanied by a second “mode” lying inside the Cont1 and therefore damped (shown by the magenta line with triangle symbols, hardly distinguishable from the magenta line with square symbols in this scale); the effect is qualitatively the same as in commensurate doped AF state [69,87]. Figure 5(a) shows how these two modes appear in the response function $\text{Im}R(\mathbf{q}, \omega)$ [we remind that the spin Green function $\text{Im}G_s^{xx}$ is related to the $\text{Im}R(\mathbf{q}, \omega)$ as given by Eq. (58)].

Above certain characteristic energy $\omega = \omega^*$, coherent quasiparticles disappear, they decay on electron-hole pairs. Technically, for $\omega > \omega^*$, solutions of the Eq. $D(\mathbf{q}, \omega) = 0$ (i.e., poles of the magnon Green functions) disappear outside the Cont2. They exist formally inside Cont2, however, the absolute values of $\text{Im}P_2(\mathbf{q}, \omega)$ are so high for corresponding \mathbf{q} and ω that there are no coherent quasiparticles inside the continuum as well. The form of the spin response function as a function of \mathbf{q}, ω is determined mainly by $\text{Im}P_l(\mathbf{q}, \omega)$, i.e., by the two-particle electron-hole response, in a way as it usually happens in itinerant-magnetism systems (when a role of polarization operator is roughly speaking played by the bare electron-hole susceptibility χ^0). The \mathbf{q} dependencies of $\text{Im}R(\mathbf{q}, \omega)$ for different ω belonging to the interval $\omega^* < \omega < \omega_c = \Delta$ are shown in Fig. 5(b). The maxima in the \mathbf{q} dependencies of $\text{Im}R(\mathbf{q}, \omega)$ for fixed ω determine the “dispersion” of these

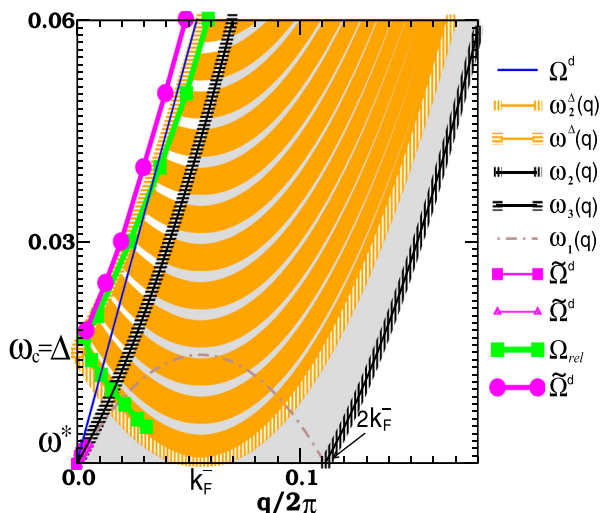


FIG. 4. The renormalized boson spectrum corresponding to the in-plane fluctuations in the (1,0) direction for the uniaxial spiral state (1,0) (calculated for the parameter values given in Sec. VI A and for the hole concentration $n = 0.04$). The magenta and green lines correspond respectively to the spectrum of resonant and relaxation type. The low-energy magenta line with square symbols corresponds to the Goldstone mode, it lies slightly above the continuum Cont1, its lower-energy counterpart mode lying inside the continuum and damped is shown by the magenta line with triangles; the two modes are hardly distinguishable in the present scale but the corresponding δ -function peaks and smooth maxima appear clearly in Fig. 5(a). The high-energy magenta line with circles corresponds to magnonlike fluctuations that can be seen as a transformation of the AF-state spin waves that get a gap due to the incommensurability of the magnetic order. The green line below ω_c corresponds to the incoherent spin excitations of the two particle electron-hole origin that are settled inside the gap in the coherent excitation spectra. Other notations are as in Figs. 2 and 3.

relaxation-type fluctuations (the green line in Fig. 4). These maxima occur near the low- q border of Cont2, this happens due to a sharp behavior of the $\text{Im}P_2$, $\text{Re}P_2$ near the continuum

borders. As a consequence, the “dispersion” of this relaxation mode follows roughly the downward dispersion of the line $\omega_2^\Delta(q)$. The intensity of this mode increases with increasing ω , as seen in Fig. 5(b).

Such a behavior occurs until the energy reaches the value $\omega_c = \Delta$. Starting from ω_c , the low- q border of Cont2 is determined by the $\omega_3^\Delta(q)$ line with the upward dispersion, and the dispersion of the relaxation “mode” follows this upward tendency. At the same time, for $\omega > \omega_c$, coherent excitations, magnons, are restored, see the magenta line with circle symbols in Fig. 4, see Ref. [93]. For the parameters used, the restored-magnon branch lies slightly above the Cont2, the spectral weight is reduced due to proximity to the continuum (see the discussion in Sec. V B); the form of $\text{Im}R(q, \omega)$ as a function of q for different ω from this energy range, is shown in Fig. 5(c). One should emphasize that under small change in parameter values, the magnon branch can move into Cont2 still remaining close to its border; in this case it keeps a resonant character but acquires a damping.

In order to compare with the experimentally observable spectra, one should plot not the spectrum of bosons but the spectrum of spin fluctuations that is displaced by $\pm \mathbf{Q}$ with respect to the boson spectrum [see Eq. (58)]. We present in Fig. 6 the in-plane spin excitation spectrum in the (1,0) direction displaced by $-Q_x \equiv -Q$. [We do not plot the inner pattern (close to \mathbf{Q}_{AF}) corresponding to the mirror reflection of the spectra at $q - Q > 0$ to $q - Q < 0$, hardly distinguishable by neutrons.]

Summarizing the obtained above features of the spin dynamics, we notice the following. (1) The presence of the characteristic energy $\omega_c = \Delta$ that separates two components with qualitatively different behavior, one with resonant magnonlike fluctuations having an upward dispersion (at $\omega > \omega_c$) and another with relaxation-type fluctuations having a downward dispersion (at $\omega < \omega_c$). (2) The two components are not crossing at \mathbf{Q}_{AF} but form in the overall dispersion a sort of a neck around energy ω_c . The neck width Δq_{neck} is proportional to Q_α (in the α direction). The characteristic energy of the neck, ω_c , is linear in Q_α as well. Herein Q_α is proportional to

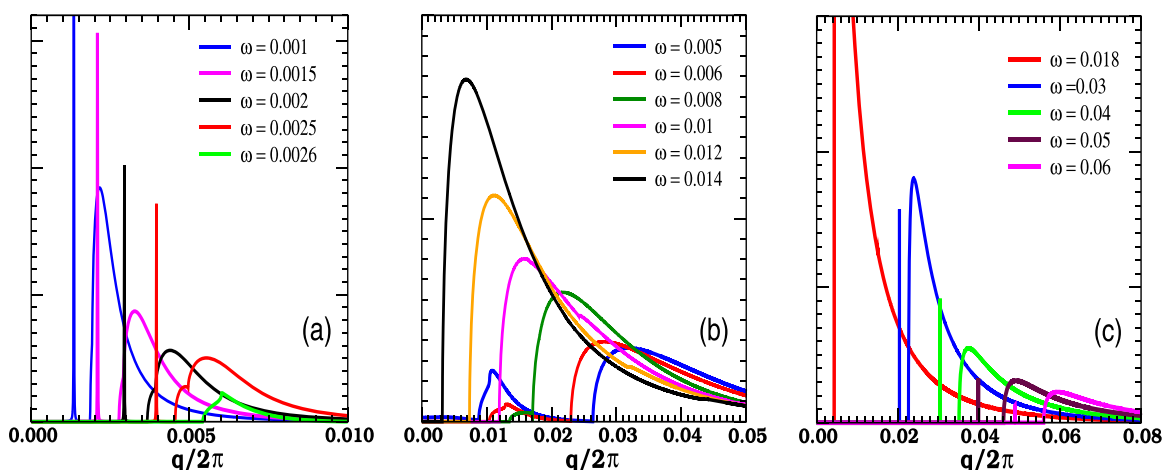


FIG. 5. Response functions $\text{Im}R(q, \omega)$, as a function of q for different intervals of ω (a) $0 < \omega < \omega^*$ (the δ -function peaks and the maxima correspond to the low-energy magenta lines in Fig. 4), (b) $\omega^* < \omega < \omega_c$ (the maxima correspond to the green line below ω_c in Fig. 4), and (c) $\omega > \omega_c$ (the δ -function peaks correspond to the magenta line with the circle symbols in Fig. 4 and the maxima correspond to the green line above ω_c). The relation of $R(q, \omega)$ to the in-plane spin Green function is given by Eq. (58).

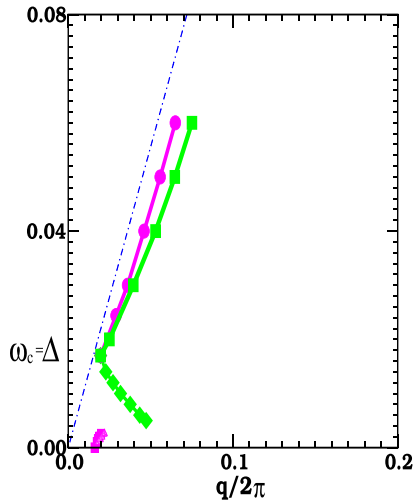


FIG. 6. Dispersion of the in-plane spin fluctuations in the (1,0) direction; the spectrum is shifted by \mathbf{Q} with respect to the boson spectrum in Fig. 4, see Eq. (58). The notations are the same as in Fig. 4. Note that the calculations have been performed with the isotropic hole spectrum ($\epsilon = 1$), i.e., with the round hole Fermi pockets, and thus the SF component below ω_c shown by the green line has a largest dispersion possible for equal other parameters, see Ref. [94]; in the opposite limit of very small ϵ corresponding to the FS strongly elongated along the $(0,\pi)$ - $(\pi,0)$ direction, the dispersion is practically vertical and the width in q is equal to Q everywhere below ω_c .

doping n if the spiral state occurs immediately upon doping or to $n - n_c^{\text{AF}}$ if it is preceded by the collinear AF state. (3) The high-energy magnonlike component can be roughly represented as a transformation of the AF-state spin waves, which get a gap due to the incommensurability of magnetic order, have a reduced spectral weight, and are accompanied for fixed ω by a continuum of two-particle fluctuations. (4) The fluctuations corresponding to the component below ω_c are anisotropic being incommensurate in one in-plane direction and commensurate in the other. They are overdamped and resemble spin excitations in itinerant-magnetism systems. Note that although this component reflects an impact of mobile holes, the spectra are not directly a spin response of doped holes: two contributions, from localized spins and mobile holes, are unified in a common structure of the Green functions more typical for localized spin systems. The incommensurability wave vector (the characteristic wave vector of this component at low energies), k_{inc} , is neither the localized-spin spiral wave vector Q nor the $2k_F$ as it would be in the metallic SDW phase. Its value depends on parameters (and then should be material dependent) but it is always much smaller than $2k_F$. The q width of the spectra decreases towards ω_c . (5) The Goldstone mode survives only at very low energies in a small area in a vicinity of $\mathbf{q} = \mathbf{Q}$, $\omega = 0$. It disappears if the spiral order is not static but quasistatic as in cuprates; however, a strong response around $\mathbf{q} = \mathbf{Q}$ should subsist at very low energies.

The described picture corresponds to the normal phase. It is, however, practically not sensitive to a presence or absence of SC order of d symmetry (the symmetry taking place in cuprates) in the case of low to moderate doping. Indeed, the mobile holes responsible for the behavior of the component

below ω_c are those near the Fermi level. At low and up to moderate doping, the Fermi pockets are small and located in the vicinity of $(\pm\pi/2, \pm\pi/2)$ where the d -wave SC gap vanishes, $\Delta^{\text{SC}}(\mathbf{k}) \rightarrow 0$. As a result, the component below ω_c is almost insensitive to the presence of SC pairing while the component above ω_c being related to localized spins is not sensitive at all. Thus the spin dynamics should not undergo a qualitative change in crossing T_c .

The obtained results are in a very good agreement with experiments for low and moderately doped cuprates [21,26–33], see also reviews [20,36]. This concerns firstly the existence of the characteristic energy ω_c , which separates two components with qualitatively different behavior. As in experiment, the component above ω_c has an upward dispersion, the spin excitations are of resonant type but have the spectral weight reduced with respect to spin waves in insulating undoped cuprates. As in experiment, the component below ω_c is quite narrow in q (see Ref. [94]) and has a slight downward dispersion, the spin excitations are anisotropic in the momentum space being incommensurate in one in-plane direction and commensurate in the other. This concerns secondly the overall form of the dispersion close to that which the experimentalists call sometimes the OPEN-hour-glass shaped sometimes Y shaped. This concerns finally the doping evolution of the characteristic energies and characteristic wave vectors, namely the monotonic increase with doping of the low-energy incommensurability, of the characteristic energy ω_c , and of the neck-width around ω_c ; for the form of the experimental spin excitation dispersion see Fig. 8(a), for the doping dependencies of certain characteristics see figures in Refs. [27,20].

On the other hand, they shed light on the difference of the behavior observed in this doping range from the archetype behavior of near-optimally-doped cuprates despite the similar in some extent form of the spin excitation dispersion in the SC state. Namely, our results explain the absence of a resonance in both normal and SC states in contrast to the near optimal doping for which the resonance is a most prominent feature of the SC-state spin dynamics, the incommensurability of the fluctuations even at ω_c for low doping versus the commensurability at ω_c for the near optimally doped SC state, the narrow dispersion of the low-energy component at low doping versus the much larger dispersion of the spin-exciton mode in the near-optimal-doping SC state, the absence of a qualitative change in the spin dynamics when crossing T_c in the former case versus the flagrant change with total disappearance of the low-energy resonant component above T_c in the latter case, and finally the different symmetries in the \mathbf{q} space of the low-energy spin excitations in the two cases.

B. Scenario for spin dynamics above critical doping n_c . Comparison of theoretical and experimental results for cuprates

As we have shown, the static ordered spiral state becomes unstable at the critical doping $n = n_c$ at which the incommensurability wave vector \mathbf{Q} reaches its critical value \mathbf{Q}_c . Experimental observations in cuprates also show a disappearance of the incommensurate magnetic order above $n = 0.08$ – 0.09 . Meanwhile, the normal-state spin dynamics observed for higher doping, i.e., for the paramagnetic (PM) state, keeps many features described in this article and corresponding to

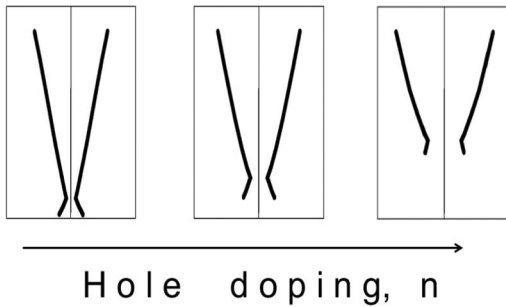


FIG. 7. Theoretical predictions for doping evolution of the normal-state spin excitation spectra in high- T_c cuprates for the paramagnetic state, $n > n_c$ (shown in a schematic way).

the ordered spiral state. This could be understood if adopting the natural hypothesis that the PM state developing above n_c preserves the spiral correlations on a finite-energy scale [that would happen in the case of the phase transition of second order, i.e., when the point $n = n_c$ is a quantum critical point (QCP)]. Such a PM state would correspond to long-lived (with a characteristic time τ_0) regions of incommensurate AF spiral correlations. The finite-energy SRO phase with local incommensuration should keep general features of the static-phase SF spectra for $\omega > \tau_0^{-1}$. On the other hand, the SFs should develop a spin gap (rather a pseudogap, see comment [95]) $\Delta^s \sim \tau_0^{-1}$.

When τ_0^{-1} (controlled by $n - n_c$) is very small, the main spin excitation features related to the two components above and below ω_c should be preserved while the Goldstone mode should disappear, see the schematic plot in Fig. 7(a). This would explain very well the normal state spin dynamics observed in $\text{YBa}_2\text{Cu}_3\text{O}_{6+x}$ (YBCO) for moderate doping (for example, for $x = 0.6$ [22–24], corresponding approximately to doping $n \sim 0.1$ – 0.12), including the absence of a resonance at ω_c , the upwardly dispersed spin excitations (reminiscent of spin waves in Neel AF) for $\omega > \omega_c$, the incommensurate spectrum with a slight downward dispersion for $\omega < \omega_c$, the small spin “gap” in the total spin response function, and finally the overall form of the dispersion.

With increasing τ_0^{-1} (increasing doping) the low-energy part of the component below ω_c should be progressively washed out. Since simultaneously the energy ω_c increases with doping, a significant part of this component should still survive, as schematically shown in Fig. 7(b). Other tendencies of doping evolution are the same as for the static spiral state since they concern the preserved part of the spin fluctuation spectrum; they are discussed in detail in the previous section.

With further increasing doping the effective gap Δ^s continues to increase and either the low-energy component is washed out completely—if Δ^s becomes at some doping higher than ω_c (that would explain the normal state spin dynamics in YBCO_7) or some part of this component around ω_c is preserved—if Δ^s remain smaller than ω_c ; this could be material dependent. The overall doping evolution of the normal-state SF spectra above n_c arising from the described above picture is shown in a schematic way in Fig. 7.

If we compare with the experimentally observed doping evolution summarized schematically in Fig. 8(b) taken from the review [36] (one should consider the normal state), the

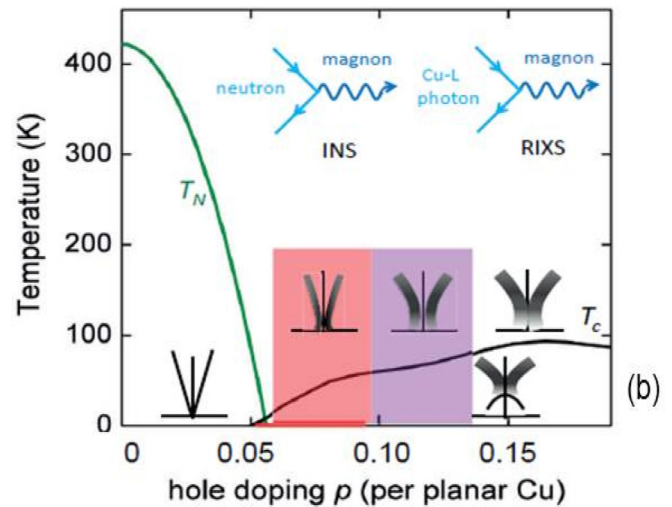
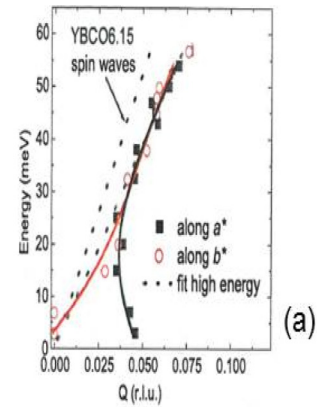


FIG. 8. Experimental neutron data for the spin-fluctuation spectra in high- T_c cuprates. (a) The SF dispersion near the AF wave vector in low-doped cuprates, namely in $\text{YBa}_2\text{Cu}_3\text{O}_{6.45}$ (reproduced from Ref. [21]). (b) Schematic summary of the doping evolution of spin dynamics through the phase diagrams in high- T_c cuprates, YBCO family (reproduced from Ref. [36]); the T_N and T_c are the AF and SC transition temperatures, the red line indicates the stability range of static incommensurate uniaxial magnetic order, the insets show the dispersion and spectral weight distribution of the SFs near the AF wave vector.

resemblance is striking. One should, however, note that in our discussion above we did not take into account the effect of the temperature, rather we tacitly assumed $T \ll \Delta^s$, which more or less corresponds to the experimental observations for the normal state of moderately and highly doped cuprates: the spin gap Δ^s measured at $T \sim 100$ K is equal to tens of meV. However, in other experimental conditions, namely in those corresponding to another T regime, the low-energy spin dynamics can be different. So, what is the role of temperature?

From a very general point of view concerning the behavior near a QCP, one can expect that the “high-energy” dynamics, for $\omega \gg T$, $\omega \gg \tau_0^{-1}$, should be qualitatively the same as for the ordered state whatever T , while the low-energy dynamics will depend on the T regime and namely on the relation between T and τ_0^{-1} . In the low- T regime, $T \ll \tau_0^{-1}$, the behavior should be qualitatively the same as that discussed above in this section, namely the SF spectrum should exhibit a gap, and moreover this gap should not change with T . In the

high- T regime, $T \gg \tau_0^{-1}$ [“quantum critical regime” (QCR)], the low-energy fluctuations should become scale invariant in space and time. The scaling description of this regime demands the renormalization group approach that is of course beyond our present scope. Although the behavior in this regime should depend on the type of system (it was studied for a very limited number of models [96]), the universal features are the disappearance of the gap and the relaxation type of dynamics. Note that in our case the critical mode is the optical mode, and therefore it is commensurate; that its low-energy part lies outside the continuum; and that the dynamical exponent $z = 1$.

For the most delicate intermediate- T regime, one could expect that the low-energy spin dynamics combines the features of the two limit regimes, namely, that the low-energy SFs are still characterized by a gap $\tilde{\Delta}^s$, whose value decreases with T , while the fluctuations immediately above this gap keep the features of QCR, i.e., are overdamped, commensurate, and satisfy scaling laws. As to the “high-energy” spin excitations, as we already told their behavior should be the same as for all other T regimes.

Coming back to cuprates. As we already emphasized, when $T \ll \Delta^s$, the spin dynamics in the PM state should be as described in the beginning of this subsection and as schematically shown in Fig. 7. For higher T , one should expect (i) for low energies—the presence of a gap and of commensurate overdamped fluctuations immediately above this gap and (ii) for high energies, $\omega \gg T$, $\omega \gg \tau_0^{-1}$, -spin dynamics qualitatively the same as for the ordered spiral state (with, of course, an additional damping of spin excitations). As to the high- T QCR regime, $T \gg \Delta^s$, it should be hardly reachable for moderately and highly doped cuprates in view of high Δ^s .

On the contrary, the QCR should be easily attainable in relatively low-doped cuprates for doping in the immediate proximity to n_c (on both sides of the QCP, $n < n_c$ and $n > n_c$, see Ref. [97]) when the $T = 0$ optical mode gap is small. Quite probably the effects observed in low-doped ($n < n_c$) cuprates, such as the persistence of low-energy excitations upon heating while, starting from $T = 150$ K, the magnetic response becomes commensurate [27,36], are fingerprints of the QCR behavior.

VII. SUMMARY AND DISCUSSION

In summary, we have studied the ordered spiral state appearing upon doping of the Mott-Neel insulator. The goal was to take into account in the most accurate way the intrinsic interrelation between spin and charge degrees of freedom in such a strongly correlated system. This study was based on the t - t' - J model with anisotropic exchange interaction. Since the t - J model was used in many ways to study the high- T_c cuprate physics, we first summarize the important points of our approach and the made approximations.

We used the representation of the Hubbard operators (HOs) via Fermi/Bose operators that is the extension of the Dyson-Maleev representation for localized spins to the algebra $Sp(1,2)$ formed by the eight HOs of the t - J model. This representation is well adapted for studying the spin dynamics of spin-charge systems with localized spin ordering, which breaks the rotational symmetry and it has several advantages

with respect to the slave-fermion/slave-boson representations. First, it preserves the local constraint between the spin and charge degrees of freedom (very important if one wishes to treat correctly the spin-charge interrelation) while in the slave-particle approaches this constraint is relaxed completely in the often used mean-field approximation, which leads to uncontrollable results. Secondly, in our representation, the spin (charge) HOs are linear in Bose (Fermi) operators in leading order while in the slave-particle representation the physical spins and charges turn out to be composite two-particle objects of auxiliary quasiparticles, spinons, and holons, so that a calculation of their (four-particle) correlation functions is an additional problem. And thirdly, the introduced by this representation Bose quasiparticles describe fluctuations above the ordered ground state, and their number is small at low T [98] so that the probability of the collisions with other Bose quasiparticles (described by high-order terms on Bose operators) tends to almost zero when $T \rightarrow 0$. (This is not so for the Bose quasiparticles introduced through the SF/SB representations: the auxiliary quasiparticles, spinons and holons, describe the ground state while the fluctuations above this ground state are the local-constraint fluctuations, which are quite difficult to treat.) Therefore, in the absence of charges ($n = 0$), we would have a quantum Bose liquid with practically undamped quasiparticles well described by the quadratic Hamiltonian. The presence of charges leads to the possibility of a decay of the boson into two fermions—a process described by the Hamiltonian $H_{s-h}^{(3)}$ and important even at $T = 0$ —moreover this process is associated with the highest energy parameter t . [When n is small (as in underdoped cuprates) one can neglect the decay into more than two fermions.]

It is the latter interaction that leads to unconventional spin dynamics that is very different from that in the doped antiferromagnetic state [69] as well as in the spiral state in insulating systems. In the latter case, such processes are simply absent; the important difference from the doped AF state arises from the fact that the fermions themselves change when the localized spin order is incommensurate: the incommensurability induces an off-diagonal order in the fermion subsystem and a gap $\Delta \propto |\mathbf{Q}|$ in the fermion spectrum. The effect arises from the kinematic spin-charge interaction and is approximation independent. The dynamic interaction with these gapped fermions leads to the unconventional \mathbf{q} and ω dependencies of the polarization operator responsible for the renormalization of the boson quasiparticle dispersion. The results are obtained by a summation of a series of bubble graphs that in the case of small n is a very good approximation. The polarization operator is calculated analytically for \mathbf{q} in a proximity to \mathbf{Q}_{AF} . The incommensurability wave vector is determined self-consistently.

For the typical for cuprates high value of the corresponding interaction constant (t), this behavior of the polarization operator results in the appearance of a gap in the *coherent* spin excitation spectrum. The upper branch of this spectrum corresponds to the magnonlike fluctuations that get a gap equal to Δ and acquire a reduced spectral weight being accompanied for fixed ω by a continuum of two-particle excitations. The lower branch of the coherent spectrum is what is left of the Goldstone mode (mandatory in the long-range ordered state as

responsible for the breaking of continuous symmetry). Being truncated by the gap from above, the Goldstone mode survives only in its initial part at very low energies. Inside the gap, incoherent spin excitations of two-particle electron-hole origin are settled. They have a slight downward dispersion (given by peaks in broad spectral densities) that roughly follows the low- q border of the gapped electron-hole continuum.

Thus globally the spin dynamics is mainly determined by the two components with qualitatively different behavior of spin excitations that are magnonlike above $\omega_c = \Delta$ and of a relaxation type below ω_c . All the details are discussed in the end of Sec. VI A. The behavior is very close to what is observed experimentally in low- and moderately-doped cuprates. The absence of the X -type crossing of the two components at \mathbf{Q}_{AF} , the absence of a resonance at ω_c , the relaxation character and the narrowness of the dispersion of the component below ω_c are the most prominent features of this spin dynamics and are contrasting with the archetype behavior in the SC state of near optimally doped cuprates. One can say that the form of the dispersion is OPEN-hour-glass-shaped since the spin excitations at ω_c remain incommensurate or that it is Y shaped because the dispersion of the component below ω_c is rather steep, see Ref. [94]. Note that the ordered state characterized by these properties is not an SDW state in an itinerant-charge system with the incommensurability wave vector $2k_F$ but the state with the spiral order of localized spins in the presence of doped holes. We emphasize again that the described spin dynamics is characteristic for both normal and SC states at low and moderate doping.

Further, we found that this ordered state becomes unstable at a certain critical doping n_c . We have argued that adopting the hypothesis about the presence of finite-energy spiral correlations in the paramagnetic state above n_c and based on the results obtained for the static spiral state, it is possible to explain practically all the details of the doping evolution of the normal-state spin dynamics in cuprates from low to high doping (compare the theoretical Fig. 7 and the experimental Fig. 8(b) above T_c). This concerns the Y -shaped form of the dispersion and the absence of a resonance in contrast to the X -shaped form and the resonance in the SC state of near optimally doped cuprates. This concerns the presence of a spin gap (our Δ^s), which in our scenario is controlled by $n - n_c$. And this concerns the persistence of high-energy magnonlike excitations observed for all doping including in the overdoped regime [99–101].

We discussed also the effect of temperature in proximity to the QCP and argued that above a certain T , the spin excitations at ω immediately above the spin gap Δ^s should be commensurate and that in the close proximity to the QCP this should happen at the lowest energies. This effect could possibly be responsible for the T behavior observed in YBCO_{6.45} [23,36] where low-energy spin excitations survive upon heating but become commensurate starting from 150 K. The latter could signal a transition to the quantum critical regime.

We hope that all these results can shed light on the origin of highly unconventional normal-state spin dynamics in cuprates. We would also like to add several words that are a speculation about the behavior in the SC state. As we mention in Ref. [95], in the metallic state above n_c in addition to the contribution related to the finite-energy spiral correlations, there is also the conventional direct hole contribution to the

spin response function. This contribution, usually small in the normal state, can be strongly enhanced in the SC state of d -wave symmetry in the way discussed in Refs. [8,10] (the spin-exciton scenario), see also Refs. [11–14]. It is important to clarify that a necessary condition for the emergence of the spin-exciton mode is the extension of the Fermi surface until or almost until the saddle-point at $(0, \pi)$ and the coherence of the charge quasiparticles in this momentum region (otherwise there is no divergence of the two-fermion response function at the electron-hole continuum border and the spin response remains weak). The spin-exciton scenario is elaborated within a pure itinerant electron approach. When both, the dynamic spiral correlations of localized spins and the static SC order are present, as on our opinion happens in the SC state of underdoped cuprates, the spin dynamics is determined by a competition between the two mechanisms and a relation between different characteristic energies. For low doping, the spin dynamics in the SC state is qualitatively the same as in the normal state, as was emphasized before, i.e., the low-energy behavior is dominated by the spiral-correlation scenario. On the other hand, starting from the near-optimal doping, the condition of the coherence of the charge quasiparticles in the near- $(0, \pi)$ region, necessary for the existence of the spin-exciton mode, is fulfilled (as known from the ARPES experiments), while the spiral correlations are weakened. As a result, for this doping range the SC-state low-energy spin dynamics should be dominated by the spin-exciton mode and the behavior as a whole should be characterized by the X -shaped dispersion in the SC state, by the resonance which disappears in the normal state, etc., (see Ref. [102]) i.e. by the archetypal behavior observed experimentally for near optimally doped cuprates. For intermediate doping, the picture should progressively change from the one limit case to the other and should be material dependent. These speculations allow one to get a qualitative insight on the overall picture of the SC-state spin dynamics in cuprates; a quantitative study of the spin dynamics resulting from the competition between the two mentioned mechanisms is beyond the scope of this article.

It is also worth mentioning certain results obtained for the charge dynamics, namely the asymmetry of the Fermi pockets with respect to the AF BZ boundary (close to that observed in certain ARPES experiment [81,82]) and especially the appearance of the off-diagonal order in the charge subsystem induced by the spiral correlations of localized spins. As shown in [83], this order has a certain relation to the so-called intra-unit-cell magnetic order observed in cuprates in the pseudogap phase [84].

As a final remark, after the submission of the manuscript, we learned about the latest neutron experiment on the HgBa₂CuO_{4+ δ} (HBCO) family of high- T_c cuprates performed for moderate [107] and near optimal doping [108]. Basically, the discovered spin dynamics fits into the theoretical scheme described in the present paper. This concerns the global shape of the spin excitation dispersion, in particular the existence of the two characteristic energies, the first (our ω_c) above which the spin excitations are magnonlike with the dispersion reminiscent of that in AF insulator but with a gap and a reduced spectral weight, and the second (our Δ^s) below which there is a global spin gap, see Fig. 4 in Ref. [107] and Fig. 11 in Ref. [108]. [The narrowness of the dispersion of the component

below ω_c in the normal state also corresponds qualitatively to our scenario although for the HBCO family the dispersion is extremely narrow, much more than for the YBCO family and namely for YBCO_{6.6} [25]. With such narrowness, of the order of the experimental resolution, it is difficult to judge whether SFs corresponding to this component are commensurate or incommensurate, whereas in YBCO_{6.6} for which the normal state spin dynamics is globally the same while the dispersion of the low-energy component is larger than the resolution, the low-energy SFs are clearly incommensurate, see, e.g., Fig. 10 in Refs. [24,25], see comments [94,109]. This concerns the absence of a resonance in the normal-state spin response. This also concerns finally the evolution of the spin dynamics with doping: for the underdoped HBCO sample, no qualitative difference between the spin dynamics in the normal and SC state was found [107], while for the near optimally doped sample, the low-energy behavior in the SC state is found to be dominated by the spin-exciton mode and very different from the normal state behavior [108]. Although the doping level in the former case is moderate rather than low, it is clear that the tendency is universal—the precise doping at which the picture corresponding to the one limit case changes for the picture corresponding to the other limit case should depend on details in the carrier band structure and other parameters and should be material dependent. [This probably is the reason why for the YBCO family the behavior in the SC state is of the optimal-doping type already for $x = 0.6$ (corresponding approximately to $n = 0.1$), while for the HBCO family, the SC-state behavior is still of the normal-state type for approximately the same n .] This is all the more so as the different families of cuprates differ by the number of CuO₂ layers, by the crystal structure and by the importance of disorder effects. The HBCO family, which is single-layered, does not have such strong disorder effects as the LSCO family and in addition has a simple tetragonal structure may reveal the most basic cuprate behavior.

ACKNOWLEDGMENTS

I am grateful to P. Pfeuty, Y. Sidis, and Ph. Bourges for stimulating discussions and comments.

APPENDIX: EXPRESSIONS FOR RENORMALIZED GREEN FUNCTIONS AND SPECTRUM OF BOSONS IN THE LIMIT $q' \sim \sqrt{2}\bar{\Delta}^c$

As seen from the expressions (50) and (51) for the scattering amplitudes M^c and M^d , in the limit $q' \sim \sqrt{2}\bar{\Delta}^c$ both amplitudes are proportional to q' , while $\frac{(M^c)^2}{(M^d)^2} \sim \frac{1}{\sqrt{1+\zeta}}$. As a result, the polarization operators Π_d^+ , Π_c^+ , Π_{cd}^+ , as well

as Π_d^- , Π_c^- , Π_{cd}^- , have the same functional dependencies and differ only by the numerical factors related to the amplitudes. In this case, one can reduce the 4×4 matrix \hat{G} to the effective 2×2 matrix \hat{G}^{eff} in the way shown below. First, we introduce the vector operators

$$\phi = \begin{bmatrix} M^d d_{\mathbf{q}} - M^c c_{-\mathbf{q}}^+ \\ M^d d_{-\mathbf{q}}^+ - M^c c_{\mathbf{q}} \end{bmatrix},$$

$$\phi^+ = (M^d d_{\mathbf{q}}^+ - M^c c_{-\mathbf{q}}, M^d d_{-\mathbf{q}} - M^c c_{\mathbf{q}}^+). \quad (\text{A1})$$

Then, the renormalized effective matrix Green function is given by

$$(\hat{G}^{\text{eff}})^{-1} = (\hat{G}^{\text{bare}})^{-1} - \hat{\Pi}^{\text{eff}}, \quad (\text{A2})$$

where \hat{G}^{bare} is the diagonal bare Green function with the components

$$G_{11}^{\text{eff}} = M_d^2 G_{dd^+} + M_c^2 G_{cc^+} = \frac{-(\alpha - \beta)}{(i\omega_n - \Omega^d)(i\omega_n + \Omega^c)} \quad (\text{A3})$$

and $G_{22}^{\text{eff}}(\mathbf{q}, i\omega_n) = G_{11}^{\text{eff}}(-\mathbf{q}, -i\omega_n)$, while $\hat{\Pi}^{\text{eff}}$ is the matrix polarization operator

$$\hat{\Pi}^{\text{eff}} = \begin{bmatrix} \Pi_{i\omega_n}^+ & -\Pi_{i\omega_n}^- \\ -\Pi_{i\omega_n}^- & \Pi_{i\omega_n}^+ \end{bmatrix}. \quad (\text{A4})$$

Above we denoted $\alpha = i\omega_n(M_c^2 - M_d^2)$, $\beta = \Omega_c M_d^2 + \Omega_d M_c^2$, $\Pi_{i\omega_n}^+ = \Pi_{11}^{\text{eff}}(\mathbf{q}, i\omega_n)$, $\Pi_{i\omega_n}^- = \Pi_{12}^{\text{eff}}(\mathbf{q}, i\omega_n)$ and took into account that $\Pi_{22}^{\text{eff}}(\mathbf{q}, i\omega_n) = \Pi_{11}^{\text{eff}}(-\mathbf{q}, -i\omega_n)$, $\Pi_{12}^{\text{eff}}(\mathbf{q}, i\omega_n) = \Pi_{21}^{\text{eff}}(-\mathbf{q}, i\omega_n)$ and $\Pi_{\mathbf{q}}^{\pm} = \Pi_{-\mathbf{q}}^{\pm}$. Then, the determinant $D_{\omega} \equiv \det(\hat{G}^{\text{eff}})$ is given on the real axis by

$$D_{\omega} = [(\Pi_{\omega}^+)^2 - (\Pi_{\omega}^-)^2](\alpha_{\omega} - \beta)(\alpha_{-\omega} - \beta)$$

$$+ \Pi_{\omega}^+[(\alpha_{\omega} - \beta)(\omega + \Omega_d)(\omega - \Omega_c)$$

$$+ (\alpha_{-\omega} - \beta)(\omega - \Omega_d)(\omega + \Omega_c)]$$

$$+ (\omega^2 - \Omega_d^2)(\omega^2 - \Omega_c^2), \quad (\text{A5})$$

above, we omit the wave vector argument in Π^{\pm} , α , β and the ω and \mathbf{q} arguments in Ω_d , Ω_c for short. By definition, this determinant is equal to the determinant of the initial 4×4 Green function (54). Note that Π_{ω}^{\pm} introduced above differ from $\Pi_{c,d}^{\pm}(\mathbf{q}, \omega)$, $\Pi_{cd}^{\pm}(\mathbf{q}, \omega)$ used in the main text only by the factors related to the scattering amplitudes. Coming back to the notations in the main text and using the polarization operators $P_{1,2}^d$ and $P_{1,2}^c$, we can explicitly write down the equations for the renormalized spectrum (given by the solutions of the equation $D_{\omega} = 0$) in a quite compact way. The explicit expressions are presented in the main text, see Eq. (75).

[1] P. Monthoux and D. Pines, *Phys. Rev. Lett.* **69**, 961 (1992).
 [2] F. Onufrieva and P. Pfeuty, *Phys. Rev. Lett.* **102**, 207003 (2009).
 [3] T. Dahm, V. Hinkov, S. V. Borisenko, A. A. Kordyuk, V. B. Zabolotnyy, J. Fink, B. Buchner, D. J. Scalapino, W. Hanke, and B. Keimer, *Nat. Phys.* **5**, 217 (2009).
 [4] F. Onufrieva and P. Pfeuty, *Phys. Rev. Lett.* **109**, 257001 (2012).
 [5] D. J. Scalapino, *Rev. Mod. Phys.* **84**, 1383 (2012).
 [6] A. V. Chubukov, *Annu. Rev. Condens. Mater. Phys.* **3**, 57 (2012).

[7] The spin-exciton mode with downward dispersion was predicted in Ref. [8], first observed experimentally in Ref. [9] and latter on discussed in many theoretical and experimental papers, see e.g., Refs. [10–13] and the review in Ref. [14] for theory and Refs. [15–19] and the review [20] for experiment.
 [8] F. Onufrieva and P. Pfeuty, [arXiv:cond-mat/9903097](https://arxiv.org/abs/cond-mat/9903097).
 [9] P. Bourges, Y. Sidis, H. F. Fong, L. P. Regnault, J. Bossy, A. Ivanov, and B. Keimer, *Science* **288**, 1234 (2000).
 [10] F. Onufrieva and P. Pfeuty, *Phys. Rev. B* **65**, 054515 (2002).

- [11] M. R. Norman, *Phys. Rev. B* **61**, 14751 (2000).
- [12] A. V. Chubukov, B. Jankó, and O. Tchernyshyov, *Phys. Rev. B* **63**, 180507(R) (2001).
- [13] I. Eremin, D. K. Morr, A. V. Chubukov, K. H. Bennemann, and M. R. Norman, *Phys. Rev. Lett.* **94**, 147001 (2005).
- [14] M. Eschrig, *Adv. Phys.* **55**, 47 (2006).
- [15] S. M. Hayden, H. A. Mook, Pengcheng Dai, T. G. Perring, and F. Dogan, *Nature (London)* **429**, 531 (2004).
- [16] J. M. Tranquada, H. Woo, T. G. Perring, H. Goka, G. D. Gu, G. Xu, M. Fujita, and K. Yamada, *Nature (London)* **429**, 534 (2004).
- [17] D. Reznik, P. Bourges, L. Pintschovius, Y. Endoh, Y. Sidis, T. Masui, and S. Tajima, *Phys. Rev. Lett.* **93**, 207003 (2004).
- [18] B. Vignolle, S. M. Hayden, D. F. McMorrow, H. M. Rønnow, B. Lake, C. D. Frost, and T. G. Perring, *Nat. Phys.* **3**, 163 (2007).
- [19] G. Xu, G. D. Gu, M. Hücker, B. Fauqué, T. G. Perring, L. P. Regnault, and J. M. Tranquada, *Nat. Phys.* **5**, 642 (2009).
- [20] M. Fujita, H. Hiraka, M. Matsuda, M. Matsuura, J. M. Tranquada, S. Wakimoto, G. Xu, and K. Yamada, *J. Phys. Soc. Jap.* **81**, 011007 (2012).
- [21] V. Hinkov, In Plane Anisotropy of the Spin-Excitation Spectrum in Tween-Free $\text{YBa}_2\text{Cu}_3\text{O}_{6+x}$, Thesis, Max-Planck-Institut für Festkörperforschung, Stuttgart, 2007.
- [22] V. Hinkov, P. Bourges, S. Pailhès, Y. Sidis, A. Ivanov, C. D. Frost, T. G. Perring, C. T. Lin, D. P. Chen, and B. Keimer, *Nat. Phys.* **3**, 780 (2007).
- [23] V. Hinkov, D. Haug, B. Fauqué, P. Bourges, Y. Sidis, A. Ivanov, C. Bernhard, C. T. Lin, and B. Keimer, *Science* **319**, 597 (2008).
- [24] V. Hinkov, C. T. Lin, M. Raichle, B. Keimer, Y. Sidis, P. Bourges, S. Pailhès, and A. Ivanov, *Eur. Phys. J. Special Topics* **188**, 113 (2010).
- [25] V. Hinkov, B. Keimer, A. Ivanov, P. Bourges, Y. Sidis, and C. D. Frost, *arXiv:1006.3278*.
- [26] D. Haug, V. Hinkov, A. Suchaneck, D. S. Inosov, N. B. Christensen, C. H. Niedermayer, P. Bourges, Y. Sidis, J. T. Park, A. Ivanov, C. T. Lin, J. Mesot, and B. Keimer, *Phys. Rev. Lett.* **103**, 017001 (2009).
- [27] D. Haug, V. Hinkov, Y. Sidis, P. Bourges, N. B. Christensen, A. Ivanov, T. Keller, C. T. Lin, and B. Keimer, *New J. Phys.* **12**, 105006 (2010).
- [28] A. Suchaneck, V. Hinkov, D. Haug, L. Schulz, C. Bernhard, A. Ivanov, K. Hradil, C. T. Lin, P. Bourges, B. Keimer, and Y. Sidis, *Phys. Rev. Lett.* **105**, 037207 (2010).
- [29] M. Enoki, M. Fujita, T. Nishizaki, S. Iikubo, D. K. Singh, S. Chang, J. M. Tranquada, and K. Yamada, *Phys. Rev. Lett.* **110**, 017004 (2013).
- [30] S. Li, Z. Yamani, H. J. Kang, K. Segawa, Y. Ando, X. Yao, H. A. Mook, and P. Dai, *Phys. Rev. B* **77**, 014523 (2008).
- [31] C. Stock, W. J. L. Buyers, R. A. Cowley, P. S. Clegg, R. Coldea, C. D. Frost, R. Liang, D. Peets, D. Bonn, W. N. Hardy, and R. J. Birgeneau, *Phys. Rev. B* **71**, 024522 (2005).
- [32] C. Stock, W. J. L. Buyers, Z. Yamani, Z. Tun, R. J. Birgeneau, R. Liang, D. Bonn, and W. N. Hardy, *Phys. Rev. B* **77**, 104513 (2008).
- [33] M. Matsuda, M. Fujita, S. Wakimoto, J. A. Fernandez-Baca, J. M. Tranquada, and K. Yamada, *Phys. Rev. Lett.* **101**, 197001 (2008).
- [34] N. B. Christensen, D. F. McMorrow, H. M. Rønnow, B. Lake, S. M. Hayden, G. Aeppli, T. G. Perring, M. Mangkorntong, M. Nohara, and H. Takagi, *Phys. Rev. Lett.* **93**, 147002 (2004).
- [35] J. M. Tranquada, C. H. Lee, K. Yamada, Y. S. Lee, L. P. Regnault, and H. M. Rønnow, *Phys. Rev. B* **69**, 174507 (2004).
- [36] Bernhard Keimer, Recent Advances in Experimental Research on High-Temperature Superconductivity in *Emergent phenomena in Correlated Matter Modeling and Simulation* (Forshungszentrum Julich, 2013), Vol. 3, p. 91.
- [37] The idea that a decrease in the kinetic energy of mobile charge carriers can offset the increase in energy of localized spins and stabilise an incommensurate spiral order was first suggested in Ref. [38].
- [38] B. I. Shraiman and E. D. Siggia, *Phys. Rev. Lett.* **62**, 1564 (1989).
- [39] J. Gan, N. Andrei, and P. Coleman, *J. Phys.: Condens. Matter* **3**, 3537 (1991).
- [40] J. I. Igarashi and P. Fulde, *Phys. Rev. B* **45**, 10419 (1992).
- [41] H. Mori and M. Hamada, *Phys. Rev. B* **48**, 6242 (1993).
- [42] A. V. Chubukov and K. A. Musaelian, *Phys. Rev. B* **51**, 12605 (1995).
- [43] P. A. Lindgard, *Phys. Rev. Lett.* **95**, 217001 (2005).
- [44] O. P. Sushkov and V. N. Kotov, *Phys. Rev. B* **70**, 024503 (2004).
- [45] D. Yoshioka, *J. Phys. Soc. Jap.* **58**, 1516 (1989).
- [46] C. Jayaprakash, H. R. Krishnamurthy, and S. Sarker, *Phys. Rev. B* **40**, 2610 (1989).
- [47] C. L. Kane, P. A. Lee, T. K. Ng, B. Chakraborty, and N. Read, *Phys. Rev. B* **41**, 2653 (1990).
- [48] B. Chakraborty, N. Read, C. Kane, and P. A. Lee, *Phys. Rev. B* **42**, 4819 (1990).
- [49] A. Auerbach and B. E. Larson, *Phys. Rev. B* **43**, 7800 (1991).
- [50] S. K. Sarker, *Phys. Rev. B* **47**, 2940(R) (1993).
- [51] L. O. Manuel and H. A. Ceccatto, *Phys. Rev. B* **61**, 3470 (2000).
- [52] When the order is not static but quasistatic, as in the magnetically ordered incommensurate phase in cuprates, this mode should disappear being replaced by a smeared spin response around $\mathbf{q} = \pm\mathbf{Q}$.
- [53] D. Petitgrand, S. V. Maleyev, Ph. Bourges, and A. S. Ivanov, *Phys. Rev. B* **59**, 1079 (1999).
- [54] S. Shamoto, M. Sato, J. M. Tranquada, B. J. Sternlieb, and G. Shirane, *Phys. Rev. B* **48**, 13817 (1993).
- [55] The relatively strong easy-plane spin anisotropy in cuprates is recently confirmed by finding in highly doped YBCO an anisotropic spin response with strong fluctuations perpendicular to the c axis [56].
- [56] N. S. Headings, S. M. Hayden, J. Kulda, N. H. Babu, and D. A. Cardwell, *Phys. Rev. B* **84**, 104513 (2011).
- [57] K. A. Chao, J. Spalek, and A. M. Oles, *J. Phys. C* **10**, L271 (1977).
- [58] C. Gros, R. Joynt, and T. M. Rice, *Phys. Rev. B* **36**, 381 (1987).
- [59] F. C. Zhang and T. M. Rice, *Phys. Rev. B* **37**, 3759 (1988).
- [60] V. I. Belinicher and A. L. Chernyshev, *Phys. Rev. B* **47**, 390 (1993); **49**, 9746 (1994).
- [61] O. K. Andersen, A. I. Liechtenstein, O. Jepsen, and F. Paulsen, *J. Phys. Chem. Sol.* **56**, 1573 (1995).
- [62] Yu. Izumov and Yu. Skryabin, *Statistical Mechanics of Magnetically Ordered Systems* (Springer-Verlag, Berlin, 1988).

- [63] S. G. Ovchinnikov and V. V. Val'kov, *Hubbard Operators in the Theory of Strongly Correlated Electrons* (Imperial College Press, London, 2004).
- [64] F. Onufrieva and J. Rossat-Mignod, *Phys. Rev. B* **52**, 7572 (1995).
- [65] Z. Zou and P. W. Anderson, *Phys. Rev. B* **37**, 627 (1988).
- [66] G. Kotliar and J. Liu, *Phys. Rev. B* **38**, 5142 (1988).
- [67] P. A. Lee and N. Nagaosa, *Phys. Rev. B* **46**, 5621 (1992).
- [68] T. Tanamoto, K. Kuboki, and H. Fukuyama, *J. Phys. Soc. Jap.* **60**, 3072 (1991).
- [69] F. P. Onufrieva, V. P. Kushnir, and B. P. Toperverg, *Phys. Rev. B* **50**, 12935 (1994).
- [70] Zhe Chang, *Phys. Rev. B* **53**, 1171 (1996).
- [71] B. S. Shastry, *Ann. Phys.* **343**, 164 (2014).
- [72] Sometimes to study spin dynamics in LRO states with spiral correlations of localized spins described by the t-J model, mixed representations are used in which the spin and charge HOs are expressed via Bose/Fermi operators in an independent way [39–41] (for example, in Ref. [39], the spin operators are expressed through the Holstein-Primakoff representation and the charge operators through the slave-fermion representation). Such mixed representations relax the interrelation between the spin and charge degrees of freedom in the complete $Spl(1,2)$ algebra.
- [73] Similar result of instability related to the out-of-plane susceptibility was found in Ref. [42] for SDW coplanar spiral state treated within the one band Hubbard model in the metallic limit.
- [74] C. L. Kane, P. A. Lee, and N. Read, *Phys. Rev. B* **39**, 6880 (1989).
- [75] Z. Liu and E. Manousakis, *Phys. Rev. B* **45**, 2425 (1992).
- [76] G. Martinez and P. Horsch, *Phys. Rev. B* **44**, 317 (1991).
- [77] R. Eder and K. W. Becker, *Z. Phys. B* **78**, 219 (1990).
- [78] E. Dagotto, A. Nazarenko, and M. Boninsegni, *Phys. Rev. Lett.* **73**, 728 (1994).
- [79] V. I. Belinicher, A. L. Chernyshev, and V. A. Shubin, *Phys. Rev. B* **54**, 14914 (1996).
- [80] T. Tohyama and S. Maekawa, *Supercond. Sci. Technol.* **13**, R17 (2000).
- [81] J. Meng, G. Liu, W. Zhang, L. Zhao, H. Liu, X. Jia, D. Mu, S. Liu, X. Dong, J. Zhang, W. Lu, G. Wang, Y. Zhou, Y. Zhu, X. Wang, Z. Xu, C. Chen, and X. J. Zhou, *Nature (London)* **462**, 335 (2009).
- [82] H. B. Yang, J. D. Rameau, Z-H. Pan, G. D. Gu, P. D. Johnson, H. Claus, D. G. Hinks, and T. E. Kidd, *Phys. Rev. Lett.* **107**, 047003 (2011).
- [83] F. Onufrieva and P. Pfeuty (unpublished).
- [84] B. Fauque, Y. Sidis, V. Hinkov, S. Pailhes, C. T. Lin, X. Chaud, and P. Bourges, *Phys. Rev. Lett.* **96**, 197001 (2006); L. Mangin-Thro, Y. Sidis, P. Bourges, S. De Almeida-Didry, F. Giovannelli, and I. Laffez-Monot, *Phys. Rev. B* **89**, 094523 (2014).
- [85] When writing the expression (54) for the matrix boson Green function we took into account the symmetry properties between different polarization-operator components and the symmetry properties of the polarization operator on the real axis: $P_l(\mathbf{q}, \omega) = P_l(-\mathbf{q}, \omega)$, $P_l(\mathbf{q}, -\omega) = (P_l(\mathbf{q}, \omega))^*$, $l=1,2$ (we omitted the superscripts “d”, “c”).
- [86] It can be shown by explicit calculations, when integrating over \mathbf{k} in the expressions for Π_d^\pm and Π_{cd}^\pm , that in the limit of small q' (namely, $q' \ll \sqrt{2}\bar{\Delta}^c$) the mixed components Π_{cd}^\pm contain the additional factor $s = \alpha \frac{\sqrt{\bar{\Delta}^c}}{\sqrt{q'}} (k_F^-/\alpha)^4$ with respect to Π_d^\pm . This factor is small when $(k_F^-)^4 \ll \sqrt{q'}/\bar{\Delta}^c$ under condition $\alpha \equiv \frac{\omega}{aq'} > \sim 1$. Note that for the Ω^d mode, one can put $\omega = \tilde{c}q'$, so that $\alpha = \tilde{c}/a \sim 1$, while for the optical mode $\alpha \gg 1$ for small q' , and thus s is small in both cases.
- [87] A. Sherman and M. Schreiber, *Phys. Rev. B* **48**, 7492 (1993).
- [88] J.-I. Igarashi and P. Fulde, *Phys. Rev. B* **45**, 12357 (1992).
- [89] These lines are exhaustive in the case when only Fermi pockets related to the $E_{\mathbf{k}}^-$ branch are filled. When the pockets related to the $E_{\mathbf{k}}^+$ branch are also filled, there are additional lines given by the expressions (81) and (82) with k_F^- replaced by k_F^+ . There are also additional lines originated from k_F^- : $\omega_1^{-\Delta}(\mathbf{q}) = a\bar{q}(2k_F^- - \bar{q}) - \Delta$, $\omega_3^{-\Delta}(\mathbf{q}) = -a\bar{q}(2k_F^- + \bar{q}) - \Delta$; in the case of $k_F^+ = 0$, they are located at negative energies.
- [90] B. O. Wells, Z. X. Shen, A. Matsuura, D. M. King, M. A. Kastner, M. Greven, and R. J. Birgeneau, *Phys. Rev. Lett.* **74**, 964 (1995).
- [91] S. La Rosa, I. Vobornik, F. Zwick, H. Berger, M. Grioni, G. Margaritondo, R. J. Kelley, M. Onellion, and A. Chubukov, *Phys. Rev. B* **56**, R525(R) (1997).
- [92] The optical boson mode Ω^c related to the out-of-plane spin excitations is much less renormalized near \mathbf{Q}_{AF} by the spin-charge interaction than the mode Ω^d related to the in-plane spin excitations, so that the dispersion of the bare mode Ω^c (shown by the violet line in Fig. 3) is roughly conserved outside the continuum. This is due to higher sensibility of the out-of-plane fluctuations to P_1 than to P_2 (as seen from the analytical expressions in Sec. V), while $|\text{Re}P_1|$ is significantly lower than $|\text{Re}P_2|$ for the relevant ω , \mathbf{q} , and especially due to the location of the bare Ω^c mode with respect to the two continua when its gap $\bar{\Delta}^c$ is high enough.
- [93] The reason for the existence of poles of the boson Green functions (or in other words of coherent quasiparticles) near the upper energy border of the Cont2 and for their absence near the lower energy border of the Cont2 is the opposite behavior of $\text{Re}P_2$ in these two cases: $\text{Re}P_2 > 0$ in the former case and $\text{Re}P_2 < 0$ in the latter case, as follows from the expressions (78).
- [94] Note that the steepness of the low-energy-component dispersion in the in-plane spin excitations depends on the mobile-hole dispersion: the higher the inverse effective mass in the hole dispersion (31) the smaller the characteristic wave vector of the continuum Cont2 with respect to k_F^- (see Fig. 2) and therefore the steeper the dispersion of this component. On the other hand, the higher the anisotropy $\epsilon = \sqrt{b/a}$ in the hole dispersion [i.e., the higher the elongation of the Fermi surface along the $(0, \pi) - (\pi, 0)$ direction] the smaller k_F^- and therefore again the steeper the dispersion of the low-energy SF component. Note that the SF spectrum in Fig. 6 was calculated with the isotropic ($\epsilon = 1$) hole dispersion (round Fermi pockets), that is, it corresponds to the largest low-energy-component dispersion possible at equal other parameters; in the opposite limit case of very small ϵ corresponding to the highly elongated FS, the dispersion is practically vertical and its width in q is equal to Q everywhere below ω_c .
- [95] For the state above n_c , Δ^s is not a true gap but a pseudogap. Indeed, this gap concerns the response function of localized spins. Doped holes although influencing strongly the form of

the latter, do not contribute directly to the spin susceptibility as far as the spiral order is static/quasistatic. On the contrary, in the metallic paramagnetic phase above n_c , the spin susceptibility contains the conventional direct contribution from mobile holes in addition to the contribution related to the finite-energy spiral correlations. However, the former contribution should be weak, as it usually happens for paramagnetic metallic systems, except for some special cases, including the case of the d-symmetry SC state where the spin response is enhanced in the way discussed in Refs. [8,10–13] (the spin-exciton scenario).

- [96] S. Sachdev, *Quantum Phase Transitions* (Cambridge University Press, Cambridge, UK, 1999).
- [97] Note that from very general understanding of the physics near QCP, the “high”-temperature regimes are the same on both sides of QCP. This of course is not the case for the low- T regimes: on the disordered side, $n > n_c$, the behavior is as described in Sec. VI B, on the ordered side, $n < n_c$, the long-range order exists only at $T = 0$ for pure 2D system and in some temperature range until $T_c(n)$ for quasi-2D system. In the latter case, there is a classical critical regime near $T_c(n)$ in some, not wide, T region, while for “high” T , the behavior is the same as on the disordered side.
- [98] The so-called zero-point fluctuations existing at $T = 0$ in the case when the ground state is generated by an operator not commuting with the Hamiltonian have usually a very small density.
- [99] M. Le Tacon, M. Minola, D. C. Peets, M. Moretti Sala, S. Blanco-Canosa, V. Hinkov, R. Liang, D. A. Bonn, W. N. Hardy, C. T. Lin, T. Schmitt, L. Braicovich, G. Ghiringhelli, and B. Keimer, *Phys. Rev. B* **88**, 020501(R) (2013).
- [100] O. J. Lipscombe, S. M. Hayden, B. Vignolle, D. F. McMorrow, and T. G. Perring, *Phys. Rev. Lett.* **99**, 067002 (2007).
- [101] S. Wakimoto, K. Yamada, J. M. Tranquada, C. D. Frost, R. J. Birgeneau, and H. Zhang, *Phys. Rev. Lett.* **98**, 247003 (2007).
- [102] Note that such a behavior was indeed found in certain microscopical theories for the paramagnetic state [103] based on decoupling schemes that have taken into account both localized-spin and itinerant-charge contributions to the spin response function. As in such decoupling schemes only *commensurate* short-range order of the localized spins was allowed and on the other hand the itinerant-charge contribution was calculated based on the free carrier dispersion [supposing coherent quasiparticles in the whole BZ and large FS extended until $(0,\pi)$ point], these theories are relevant only for the near optimal doping. Similar approaches based on the Mori projection technique with the similar approximations and therefore having the same restrictions have been used in Refs. [104–106]. In the early microscopical work [64] where the dual localized-itinerant nature of spin excitations in cuprates has probably been considered for the first time, the incommensurate short-range order of localized spins was allowed but the electron-hole contribution was also calculated based on the free carrier dispersion that again limits the applicability of the theory to the region of near optimal doping.
- [103] M. V. Eremin, I. M. Shigarev, and I. M. Eremin, *Eur. Phys. J.* **85**, 131 (2012).
- [104] A. Sherman and M. Schreiber, *Phys. Rev. B* **68**, 094519 (2003).
- [105] A. A. Vladimirov, D. Ihle, and N. M. Plakida, *Phys. Rev. B* **83**, 024411 (2011).
- [106] P. Prelovsek and I. Sega, *Phys. Rev. B* **74**, 214501 (2006).
- [107] M. K. Chan, C. J. Dorow, L. Mangin-Thro, Y. Tang, Y. Ge, M. J. Veit, G. Yu, X. Zhao, A. D. Christianson, J. T. Park, Y. Sidis, P. Steffens, D. L. Abernathy, Ph. Bourges, and M. Greven, *Nature Commun.* **7**, 10819 (2016).
- [108] M. K. Chan, Y. Tang, C. J. Dorow, J. Jeong, L. Mangin-Thro, M. J. Veit, Y. Ge, D. L. Abernathy, Y. Sidis, Ph. Bourges, and M. Greven, *Phys. Rev. Lett.* **117**, 277002 (2016).
- [109] When comparing with experiment one should take into account that in addition to the in-plane spin excitations there are also the out-of-plane spin excitations that are commensurate. It seems that in the cited neutron experiments [107,108], the measured response function is a superposition of the two types of excitations. Then, the measured below ω_c spin fluctuations are a superposition of the commensurate out-of-plane and incommensurate in-plane excitations, so that in the experimental spectra the incommensurability of the in-plane excitations should rather appear as a q width of these superposed excitations.